Unified Model for NO_x Absorption in Aqueous Alkaline and Dilute Acidic Solutions

Janaki A. Patwardhan and Jyeshtharaj B. Joshi
Institute of Chemical Technology, University of Mumbai, Matunga, Mumbai 400 019, India

The absorption of NO_X gases in water and alkalies [NaOH, NH_4OH, $Ca(OH)_2$)] provides commercially important products nitric acid and salts (nitrates and nitrites), respectively. This complex phenomena of mass transfer with chemical reactions is described quantitatively in terms of $[H_\sqrt{(kD)}]_J$ values for J = N_2O_3, N_2O_4. However, the reported value of $H_\sqrt{(kD)}$ for N_2O_3 absorption in strong alkaline solution was 50 times its value in water. For the intermediate case of NO_X absorption in weak alkali $Ca(OH)_2$, it was necessary to have a mathematical model which incorporated the HNO_2 decomposition, as well as neutralization by alkali. This led to a unified model for NO_X absorption, which can be used for predicting point rates of NO_X absorption as well as selectivity, for various gas compositions and liquid-phase pH. Parametric sensitivity has been reported. A comparison of the model predictions with data from patent on $Ca(NO_2)_2$ manufacture has been made to test the model validity.

Introduction

The continual research on absorption of oxides of nitrogen (NO_X) in the past 85 years is driven by: (a) the scientific fervor to comprehend this complex, multicomponent system in terms of kinetics and thermodynamics, (b) its commercial relevance in production of nitric acid, nitrates, nitrites, and so on, and (c) the need to design NO_X pollution abatement facilities.

The oxides of nitrogen (NO_X) denote a mixture of gases NO, NO_2, N_2O_3, N_2O_4, HNO_2, and HNO_3. The absorption of NO_X gases in water and alkalies [NaOH, NH_4OH, $Ca(OH)_2$)] provides commercially important products nitric acid and salts (nitrates and nitrites), respectively. The liquid phase contains the dissolved, as well as ionized species NO, NO_2, N_2O_3, N_2O_4, HNO_2, H^+, OH^-, NO_2^-, NO_3^-, and metal cation (Ca^{++}, Na^+). Thus, there are many components in the gas and liquid phases. They simultaneously undergo chemical reactions among themselves during the absorption process. Thus, NO_X absorption is complex. An improved understanding of this system helps to visualize the NO_X absorption process and model it in mathematical terms. A generic model can serve as a tool in the design and optimization of various wet processes involving NO_X.

Nitric acid is one of the top bulk chemicals produced in the world and NO_X absorption in water is an important step in the production of nitric acid. Hence, various aspects of the NO_X–water system have been studied extensively in the past (Chambers and Sherwood, 1937; Wendel and Pigford, 1958; Komiyama and Inoue, 1978, 1980; Shadid and Handley, 1990). Schwartz and White (1981) have reviewed the solubility and equilibria of the NO_X components relevant to absorption. The solubility in water varies typically in the following order $NO < NO_2 < N_2O_3 < N_2O_4 < HNO_2 < HNO_3$. Although mass transfer of all the species occurs across the gas-liquid interface, the dominant species involved in the NO_X absorption process depends on the gas and liquid compositions, temperature, and so on.

Figure 1 shows how the various reactions contribute to the pool of various molecules/ions in liquid phase. The liquid phase hydrolysis of N_2O_3 and N_2O_4 occurs rapidly in the liquid film. When the mass transfer of a species J is accompanied by an *irreversible*, first-order, chemical reaction which goes to completion within the liquid film itself, the overall rate of absorption of these species is enhanced by chemical

Correspondence concerning this article should be addressed to J. B. Joshi.

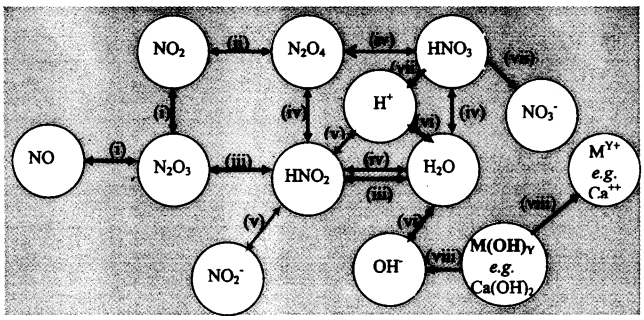

Figure 1. Contribution of the various reactions to the pool of different species in the liquid phase.

reaction (Doraiswamy and Sharma, 1984) and is conventionally expressed by

$$(R_J) = H_J\sqrt{(k_J D_J)}\,P_J^I \qquad (1)$$

In the past, various workers have studied NO_X absorption in water and alkaline solutions. Assuming that the reaction is of first order with respect to the solute, they reported the values of a lumped parameter $[H_J\sqrt{(kD)}]_J$ for $J = N_2O_3, N_2O_4$. There is little effect of alkali concentration on the $[H_J\sqrt{(kD)}]$ value for N_2O_4 absorption. In the case of N_2O_3 absorption, however, the $[H_J\sqrt{(kD)}]$ value increases by about two orders of magnitude, in strong alkaline solutions, in comparison to water (refer to Tables 1a and 1b). Aoki et al. (1982), Newman and Carta (1988), and Katima et al. (1992) have explained the reasons for the same. When NO_X is absorbed in water, then the hydrolysis of N_2O_3 is reversible, in reality, and leads to lowering of the N_2O_3 absorption rate. Moreover, the decomposition of HNO_2 and desorption of its products can also take place, leading to lower NO_X removal efficiency. However, in the presence of alkali, OH^- ions neutralize the HNO_2 (product of N_2O_3 hydrolysis) to form NO_2^- and deter the decomposition of HNO_2. As long as the OH^- is in excess and is present throughout the liquid film, the HNO_2 decomposition is minimal. Hence, the reported value of $[H_J\sqrt{(kD)}]_J$ for $J = N_2O_3$, in strong alkali, may be considered to be closer to the true value when the reverse reaction has been suppressed. The reported value of $[H_J\sqrt{(kD)}]_J$ for $J = N_2O_3$, in water is a *lumped parameter* value, due to the occurrence of the reverse of the hydrolysis reaction and N_2O_3 decomposition. There is a need for a model, which includes the kinetics of HNO_2 decomposition in the liquid phase. This aspect is also relevant to the absorption process for nitric acid manufacture.

Pradhan and Joshi (1999) have provided strategies for achieving high selectivity of sodium nitrite over nitrate by absorption of a suitably oxidized NO_X gas in strong NaOH solutions. $Ca(OH)_2$ is a cheaper alkali than NaOH in terms of cost per k-ion OH^- provided. Calcium nitrite can replace sodium nitrite in some applications. Calcium nitrite, if produced selectively, has a market value as corrosion inhibitor

Table 1a. $[H_J\sqrt{(kD)}]$ for N_2O_3

Reference	Liquid Phase	T, K	$[H_J\sqrt{(kD)}]$ for N_2O_3 kmol/m^2/s/(N/m^2)	Ref.
Hofmesiter and Kolhaas (1965)	Water		4.93×10^{-8}	Newman and Carta (1988)
Corriveau (1971)	Water	298	1.57×10^{-8}	Newman and Carta (1988)
Sherwood et al. (1975)	Water		1.63×10^{-8}	Aoki et al. (1982)
Aoki et al. (1982)	NaOH & buffer solutions	288	1.07×10^{-6}	Aoki et al. (1982)
Newman and Carta (1988)	NaOH	298	2.47×10^{-7}	Newman and Carta (1988)
		313	1.18×10^{-7}	

Table 1b. $[H_J\sqrt{(kD)}]$ for N_2O_4

Reference	Liquid Phase	T, K	$[H_J\sqrt{(kD)}]$ for N_2O_4 kmol/m^2/s/(N/m^2)	Cited From
Komiyama and Inoue (1980)	Water	288	1.4×10^{-8}	Komiyama and Inoue (1980)
Kameoka (1977)	Water	298	6.7×10^{-9}	Komiyama and Inoue (1980)
Kramers (1961)	Water	293	7.6×10^{-9}	Komiyama and Inoue (1980)
Dekker (1959)	Water	298	1.1×10^{-8}	Komiyama and Inoue (1980)
Wendel and Pigford (1958)	Water	298	5.7×10^{-9}	Komiyama and Inoue (1980)
Dekker (1959)	Water	298	1.1×10^{-8}	Werner et. al (1990)
Kramers (1961)	Water	293	7.6×10^{-9}	Werner et. al (1990)
		303	8.8×10^{-9}	Werner et. al (1990)
Werner et al. (1990)	HNO_3			Werner et. al (1990)
	15%w	298	4.7×10^{-9}	Werner et. al (1990)
	30%w	298	2.9×10^{-9}	Werner et. al (1990)
	50%w	298	1.0×10^{-9}	Werner et. al (1990)
	60%w	298	1.5×10^{-10}	Werner et. al (1990)

and antifreeze agent in the preparation of concreting mixtures for construction. However, the obstacle in the efficient production of $Ca(NO_2)_2$ is the low solubility of $Ca(OH)_2$ in water which poses a challenge to ensure conditions for high selectivity and production rate. One of the specific directions of the present work was modeling the manufacture of calcium nitrite by absorption of the polluting NO_X gases into $Ca(OH)_2$ slurry. It was required to develop a mathematical model for NO_X absorption in $Ca(OH)_2$ (pH $\cong$ 12) with the twin objectives of pollution abatement and selective manufacture of calcium nitrite. It was apparent that if the value of $[H\sqrt{(kD)}]_J$ for $J = N_2O_3$ in strong NaOH (pH $\cong$ 14) was used, then it could overpredict the rate of NO_X removal, as well as selectivity. If the value of $[H\sqrt{(kD)}]_J$ for $J = N_2O_3$ in water (pH = 7) (which was about 50 times lower than the previous value!) was used, then it could underpredict the rate of NO_X removal, as well as selectivity. As the variation was too large, it was necessary to incorporate all the real rate processes taking place in the liquid phase (especially in the liquid film) in detail to get a qualitative, as well as a quantitative, picture of the absorption process.

On the whole, a need for a generalized model to depict NO_X absorption in aqueous solutions over a wide range of OH^- concentrations was sensed. This model is described below.

Unified Model

Objective

The objective of this model (*based on two-film theory*) is to find out the point rates of NO_X removal, given specified gas and liquid bulk concentrations, temperature, pressure, liquid side mass-transfer coefficient (k_L), and gas side mass-transfer coefficient (k_G). If the concentration profiles of the various components in the gases and liquid film are known, then the absorption rates can be obtained. From the point rates, the selectivity of NO_2^- formation over NO_3^- formation can be calculated. The total rate of NO_X removal can also be calculated.

Reactions in the gas film

The gas-phase reactions, considered in the model, are given below

$$2NO(g) + O_2(g) \xrightarrow{k_1} 2NO_2(g) \quad (2)$$

$$2NO_2(g) \underset{k_{2B}}{\overset{k_{2F}}{\rightleftharpoons}} N_2O_4(g) \quad (3)$$

$$NO(g) + NO_2(g) \underset{k_{3B}}{\overset{k_{3F}}{\rightleftharpoons}} N_2O_3(g) \quad (4)$$

$$N_2O_3(g) + H_2O(g) \underset{k_{4B}}{\overset{k_{4F}}{\rightleftharpoons}} 2HNO_2(g) \quad (5)$$

$$N_2O_4(g) + H_2O(g) \underset{k_{5B}}{\overset{k_{5F}}{\rightleftharpoons}} HNO_2(g) + HNO_3(g) \quad (6)$$

Corresponding to Eqs. 2–6, the kinetic rate expressions are given in Eqs. 7–11 respectively, in Table 2.

Table 2. Rate Expressions for Gas-Phase Reactions

Rate Expression	Eq.
$-\frac{d}{dt}[NO(g)] = k_1[NO(g)]^2[O_2(g)] = A'$	7
$-\frac{d}{dt}[NO_2(g)] = k_{2F}[NO_2(g)]^2 - k_{2B}[N_2O_4(g)] = B'$	8
$-\frac{d}{dt}[NO(g)] = k_{3F}[NO(g)][NO_2(g)] - k_{3B}[N_2O_3(g)] = C'$	9
$-\frac{d}{dt}[N_2O_3(g)] = k_{4F}[N_2O_3(g)][H_2O(g)] - k_{4B}[HNO_2(g)]^2 = D'$	10
$-\frac{d}{dt}[N_2O_4(g)] = k_{5F}[N_2O_4(g)][H_2O(g)]$ $-k_{5B}[HNO_2(g)][HNO_3(g)] = M'$	11

Reactions in the liquid film

$$2NO_2(aq) \underset{k_{32B}}{\overset{k_{32F}}{\rightleftharpoons}} N_2O_4(aq) \quad (12)$$

$$NO(aq) + NO_2(aq) \underset{k_{33B}}{\overset{k_{33F}}{\rightleftharpoons}} N_2O_3(aq) \quad (13)$$

$$N_2O_3(aq) + H_2O(l) \underset{k_{34B}}{\overset{k_{34F}}{\rightleftharpoons}} 2HNO_2(aq) \quad (14)$$

$$N_2O_4(aq) + H_2O(l) \underset{k_{35B}}{\overset{k_{35F}}{\rightleftharpoons}} HNO_2(aq) + H^+(aq) + NO_3^-(aq) \quad (15)$$

The dissociation of nitrous acid and water has been incorporated

$$HNO_2(aq) \underset{k_{36B}}{\overset{k_{36F}}{\rightleftharpoons}} H^+(aq) + NO_2^-(aq) \quad (16)$$

$$H_2O(aq) \underset{k_{37B}}{\overset{k_{37F}}{\rightleftharpoons}} H^+(aq) + OH^-(aq) \quad (17)$$

Corresponding to Eqs. 12–17, the kinetic rate expressions are given in Eqs. 18–23, respectively, in Table 3.

The two equilibria (reactions shown in Eqs. 16 and 17) have been assumed to be attained instantaneously. Thus, $J' = 0$

Table 3. Rate Expressions for Liquid-Phase Reactions

Rate Expression	Eq.
$-\frac{d}{dt}[NO_2(aq)] = k_{32F}[NO_2(aq)]^2 - k_{32B}[N_2O_4(aq)] = F'$	18
$-\frac{d}{dt}[NO(aq)] = k_{33F}[NO(aq)][NO_2(aq)] - k_{33B}[N_2O_3(aq)] = G'$	19
$-\frac{d}{dt}[N_2O_3(aq)] = k_{34F}[N_2O_3(aq)] - k_{34B}[HNO_2(aq)]^2 = H'$	20
$-\frac{d}{dt}[N_2O_4(aq)] = k_{35F}[N_2O_4(aq)]$ $-k_{35B}[HNO_2(aq)][H^+(aq)][NO_3^-(aq)] = I'$	21
$-\frac{d}{dt}[HNO_2(aq)] = k_{36F}[HNO_2(aq)]$ $-k_{36B}[H^+(aq)][NO_2^-(aq)] = J'$	22
$-\frac{d}{dt}[H_2O(l)] = k_{37F}[H_2O(l)] - k_{37B}[H^+(aq)][OH^-(aq)] = K'$	23

and $K' = 0$ in Eqs. 22 and 23, respectively. Hence

$$\frac{[H^+(aq)][NO_2^-(aq)]}{[HNO_2(aq)]} = K_{36} = \frac{k_{36F}}{k_{36B}} \tag{24}$$

$$\frac{[H^+(aq)][OH^-(aq)]}{[H_2O(l)]} = \frac{k_{37F}}{k_{37B}} \tag{25}$$

$$[H^+(aq)][OH^-(aq)] = \frac{k_{37F}}{k_{37B}}[H_2O(l)] \approx \text{constant} = K_{37} \tag{26}$$

The alkali (if any) present in the dissolved form in the aqueous phase is assumed to be completely dissociated; so nitric acid is also (being a strong acid)

$$M(OH)_Y(aq) \xrightarrow{\text{instantaneous}} M^{Y+}(aq) + Y OH^-(aq) \tag{27}$$

For example, for NaOH, $Y = 1$, whereas, for $Ca(OH)_2$, $Y = 2$

$$HNO_3(aq) \rightarrow H^+(aq) + NO_3^-(aq) \tag{28}$$

It may be noted that HNO_3 dissociation is a reversible reaction (Schwartz and White, 1981). However, in dilute acidic solutions, most of the nitric acid is present in the dissociated form. In such a situation, the small concentration of undissociated HNO_3 in the aqueous phase is negligible.

Mass transfer accompanied by chemical reaction, in the gas film

The conservation equation for every species is written in terms of diffusion and chemical reaction

$$D^G_{NO}\frac{d^2}{dx_G^2}[NO(g)] - A' - C' = 0 \tag{29}$$

$$D^G_{NO_2}\frac{d^2}{dx_G^2}[NO_2(g)] + A' - C' - B' = 0 \tag{30}$$

$$D^G_{N_2O_3}\frac{d^2}{dx_G^2}[N_2O_3(g)] + C' - D' = 0 \tag{31}$$

$$D^G_{N_2O_4}\frac{d^2}{dx_G^2}[N_2O_4(g)] + B'/2 - M' = 0 \tag{32}$$

$$D^G_{O_2}\frac{d^2}{dx_G^2}[O_2(g)] - A'/2 = 0 \tag{33}$$

$$D^G_{H_2O}\frac{d^2}{dx_G^2}[H_2O(g)] - D' - M' = 0 \tag{34}$$

$$D^G_{HNO_2}\frac{d^2}{dx_G^2}[HNO_2(g)] + 2D' + M' = 0 \tag{35}$$

$$D^G_{HNO_3}\frac{d^2}{dx_G^2}[HNO_3(g)] + M' = 0 \tag{36}$$

Mass transfer accompanied by chemical reaction, in the liquid film

$$D^L_{NO}\frac{d^2}{dx_L^2}[NO(aq)] - E' - G' = 0 \tag{37}$$

$$D^L_{NO_2}\frac{d^2}{dx_L^2}[NO_2(aq)] + E' - F' - G' = 0 \tag{38}$$

$$D^L_{N_2O_3}\frac{d^2}{dx_L^2}[N_2O_3(aq)] + G' - H' = 0 \tag{39}$$

$$D^L_{N_2O_4}\frac{d^2}{dx_L^2}[N_2O_4(aq)] + F'/2 - I' = 0 \tag{40}$$

$$D^L_{O_2}\frac{d^2}{dx_L^2}[O_2(aq)] - E'/2 = 0 \tag{41}$$

$$D^L_{HNO_2}\frac{d^2}{dx_L^2}[HNO_2(aq)] + 2H' + I' - J' = 0 \tag{42}$$

$$D^L_{H^+}\frac{d^2}{dx_L^2}[H^+(aq)] + I' + J' + K' = 0 \tag{43}$$

$$D^L_{OH^-}\frac{d^2}{dx_L^2}[OH^-(aq)] + K' = 0 \tag{44}$$

$$D^L_{M^{Y+}}\frac{d^2}{dx_L^2}[M^{Y+}(aq)] = 0 \tag{45}$$

$$D^L_{NO_2^-}\frac{d^2}{dx_L^2}[NO_2^-(aq)] + J' = 0 \tag{46}$$

$$D^L_{NO_3^-}\frac{d^2}{dx_L^2}[NO_3^-(aq)] + I' = 0 \tag{47}$$

Connecting the interface concentrations of gas and liquid

Eight gas-phase interfacial partial pressures

$$P^I_{NO}, P^I_{NO_2}, P^I_{N_2O_3}, P^I_{N_2O_4}, P^I_{O_2}, P^I_{H_2O}, P^I_{HNO_2}, P^I_{HNO_3}$$

Eleven liquid side interfacial concentrations

$$[NO(aq)]^*, [NO_2(aq)]^*, [N_2O_3(aq)]^*, [N_2O_4(aq)]^*, [HNO_2(aq)]^*, [O_2(aq)]^*, [H^+(aq)]^*, [OH^-(aq)]^*, [M^{Y+}(aq)]^*, [NO_2^-(aq)]^*, [NO_3^-(aq)]^*$$

It is desired to calculate the 11 liquid-phase concentrations from the eight gas-phase partial pressures at the interface. The connecting equations are given in Table 4. Thus, there are 11 equations (Eqs. 48–58) for 11 unknown liquid concentrations. Equations 48–54 are straightforward, that is, the liquid-phase interfacial concentrations in these equations can be calculated explicitly from the gas-phase partial pressures. The balance 4 algebraically Eqs. 55–58 are solved for the four unknowns as $[H^+]^*$, $[OH^-]^*$, $[NO_2^-]^*$ and $[NO_3^-]^*$.

Table 4. Equations Connecting the Gas and Liquid Composition at the Interface

Relating Eq.	Eq.
$[NO(aq)]^* = H_{NO} P^I_{NO}$	48
$[NO_2(aq)]^* = H_{NO_2} P^I_{NO_2}$	49
$[N_2O_3(aq)]^* = H_{N_2O_3} P^I_{N_2O_3}$	50
$[N_2O_4(aq)]^* = H_{N_2O_4} P^I_{N_2O_4}$	51
$[HNO_2(aq)]^* = H_{HNO_2} P^I_{HNO_2}$	52
$[O_2(aq)]^* = H_{O_2} P^I_{O_2}$	53
$[M^{Y+}(aq)]^* = [M^{Y+}(aq)]^B$	54
$[H^+(aq)]^*[OH^-(aq)]^* = K_{37}$	55
$[H^+(aq)]^*[NO_3^-(aq)]^*/P_{HNO_3} = K_{42}$	56
$\dfrac{[H^+(aq)]^*[NO_2^-(aq)]^*}{[HNO_2(aq)]^*} = K_{36}$	57
Charge balance: $\dfrac{[H^+(aq)]^* + Y[M^{Y+}(aq)]^*}{[OH^-(aq)]^* + [NO_2^-(aq)]^* + [NO_3^-(aq)]^*} = 1$	58

Connecting the component fluxes at the gas liquid interface

The method of arriving at the interfacial liquid concentrations is shown in the preceding section. The concentration gradients at the interface are calculated as follows. Let ϕ_I denote the flux of component I at the interface, leaving the gas-phase, into the liquid phase. Let ψ_I denote the flux of component I entering into the liquid phase, at the interface

$$\phi_I = -D_I^G \frac{d}{dx_G}[I(g)]|_{X_G=\delta_G} \tag{59}$$

where $I = NO, NO_2, N_2O_3, N_2O_4, O_2, H_2O, HNO_2, HNO_3$

$$\psi_I = -D_I^L \frac{d}{dx_L}[I(aq)]|_{X_L=0} \tag{60}$$

where $I = NO, NO_2, N_2O_3, N_2O_4, O_2, HNO_2, H^+, OH^-, Ca^{++}, NO_2^-, NO_3^-$.

Then, knowing the eight values of the gas side flux (NO, O_2, N_2O_3, N_2O_4, O_2, H_2O, HNO_2, HNO_3), it is desired to find out the 11 values of the liquid side flux. However

$$\psi_{M^{Y+}} = -D^L_{M^{Y+}} \frac{d}{dx_L}[M^{Y+}(aq)]|_{X_L=\delta_L} = 0 \tag{61}$$

Thus, the values of 10 (remaining) connecting fluxes are required.

For the case of fluxes of NO, NO_2, N_2O_3, N_2O_4, and O_2

$$\psi_I = \phi_I \tag{62}$$

Thus, values of 5 (remaining) connecting fluxes are required (H^+, OH^-, HNO_2, NO_2^-, NO_3^-).

Since all the HNO_3 entering from the gas side is dissociated into H^+ and NO_3^- (note, in the assumptions, undissociated liquid-phase concentration $HNO_3 = 0$), it follows that

$$\psi_{NO_3^-} = \phi_{HNO_3} \tag{63}$$

$$-\frac{D^L_{NO_3^-}}{\Delta x_L}\{[NO_3^-(aq)] - [NO_3^-(aq)]^*\} = \phi_{HNO_3} \tag{64}$$

Thus

$$[NO_3^-(aq)] = [NO_3^-(aq)]^* - \phi_{HNO_3}\frac{\Delta x_L}{D^L_{NO_3^-}} \tag{65}$$

Thus, four fluxes remain to be connected, for HNO_2, H^+, OH^- and NO_2^-.

Since HNO_2 remains undissociated or dissociated in the liquid phase

$$\phi_{HNO_2} = \psi_{HNO_2} + \psi_{NO_2^-} \tag{66}$$

H balance gives

$$2\phi_{H_2O} + \phi_{HNO_2} + \phi_{HNO_3} = \psi_{HNO_2} + \psi_{H^+} + \psi_{OH^-} + 2\psi_{H_2O} \tag{67}$$

Since water is in large excess in the liquid phase, the small change in the liquid phase water concentration near the interface, on account of the water flux entering from gas side, has been neglected. Since the OH^- is generated from water dissociation, only

$$\phi_{H_2O} = \psi_{OH^-} + \psi_{H_2O} \tag{68}$$

Equation 67 − 2 × Eq. 68 − Eq. 66 + Eq. 63 gives

$$\psi_{NO_2^-} + \psi_{NO_3^-} + \psi_{OH^-} - \psi_{H^+} = 0 \tag{69}$$

Equations 66 and 69 are solved along with the equilibrium constraints of water dissociation and HNO_2 dissociation (Eqs. 26 and 24). At $x = \Delta x_L$, let

$$Z = [H^+(aq)] \tag{70}$$

and

$$W = [HNO_2(aq)] \tag{71}$$

Then

$$[OH^-(aq)] = K_{37}/[H^+(aq)] = K_{37}/Z \tag{72}$$

$$[NO_2^-(aq)] = K_{36}[HNO_2]/[H^+(aq)] = K_{36}W/Z \tag{73}$$

From Eq. 66

$$\phi_{HNO_2} = -D^L_{HNO_2}\frac{1}{\Delta x_L}\{[HNO_2(aq)] - [HNO_2(aq)]^*\} - D^L_{NO_2^-}\frac{1}{\Delta x_L}\{[NO_2^-(aq)] - [NO_2^-(aq)]^*\} \tag{74}$$

$$\phi_{HNO_2} = -D^L_{HNO_2}\frac{1}{\Delta x_L}\{W - [HNO_2(aq)]^*\} - D^L_{NO_2^-}\frac{1}{\Delta x_L}\{K_{36}W/Z - [NO_2^-(aq)]^*\} \tag{75}$$

$$\left(\phi_{HNO_2} - \frac{1}{\Delta x_L} D^L_{HNO_2}[HNO_2(aq)]^* - \frac{1}{\Delta x_L} D^L_{NO_2^-}[NO_2^-(aq)]^*\right) = -\left(D^L_{HNO_2}\frac{1}{\Delta x_L}\right)W - \left(D^L_{NO_2^-}\frac{1}{\Delta x_L}K_{36}\right)\frac{W}{Z} \quad (76)$$

which is of the form

$$A_2 = -\left(B_2 + \frac{C_2}{Z}\right)W \quad (77)$$

$$W = -\frac{A_2 Z}{B_2 Z + C_2} \quad (78)$$

Elaborating Eq. 69 gives

$$-\frac{1}{\Delta x_L} D^L_{NO_2^-}\{[NO_2^-(aq)] - [NO_2^-(aq)]^*\} - \frac{1}{\Delta x_L} D^L_{NO_3^-}\{[NO_3^-(aq)] - [NO_3^-(aq)]^*\} - \frac{1}{\Delta x_L} D^L_{OH^-}\{[OH^-(aq)] - [OH^-(aq)]^*\} + \frac{1}{\Delta x_L} D^L_{H^+}\{[H^+(aq)] - [H^+(aq)]^*\} = 0 \quad (79)$$

$$D^L_{NO_2^-}\{[NO_2^-(aq)] - [NO_2^-(aq)]^*\} + D^L_{NO_3^-}\{[NO_3^-(aq)] - [NO_3^-(aq)]^*\} + D^L_{OH^-}\{[OH^-(aq)] - [OH^-(aq)]^*\} - D^L_{H^+}\{[H^+(aq)] - [H^+(aq)]^*\} = 0 \quad (80)$$

At this juncture, it is also necessary to discuss that the solution to the coupled equations (Eqs. 66, 80, 26 and 22) may lead to a discrepancy in the charge balance at the point $x = \Delta x_L$, and, thus, imply a charge gradient at the interface! This problem of electropotential gradient encountered in the formulation of problems involving charged diffusing species has been brought out and treated judiciously by Brogren and Karlsson (1997) and Taylor and Krishna (1993).

The equations of charge balance at the interface and at $x = \Delta x_L$ are

$$[H^+(aq)]^* + Y[M^{Y+}(aq)]^* - [OH^-(aq)]^* - [NO_2^-(aq)]^* - [NO_3^-(aq)]^* = 0 \quad (81)$$

$$[H^+(aq)] + Y[M^{Y+}(aq)] - [OH^-(aq)] - [NO_2^-(aq)] - [NO_3^-(aq)] = 0 \quad (82)$$

Equation 81 − 82 gives

$$[NO_2^-(aq)] - [NO_2^-(aq)]^* + [NO_3^-(aq)] - [NO_3^-(aq)]^* + [OH^-(aq)] - [OH^-(aq)]^* - \{H^+(aq)] - [H^+(aq)]^*\} + \{Y[M^{Y+}(aq)] - [M^{Y+}(aq)]^*\} = 0 \quad (83)$$

Since $[M^{Y+}(aq)] = [M^{Y+}(aq)]^*$, the above equation simplifies to

$$\{[NO_2^-(aq)] - [NO_2^-(aq)]^*\} + \{[NO_3^-(aq)] - [NO_3^-(aq)]^*\} + \{[OH^-(aq)] - [OH^-(aq)]^*\} - \{[H^+(aq)] - [H^+(aq)]^*\} = 0 \quad (84)$$

A comparison of Eqs. 80 and 84 shows that they are similar in nature, except that there are different coefficients viz. $D_{NO_2^-}$, $D_{NO_3^-}$, D_{OH^-}, D_{H^+} in Eq. 80. If Eq. 80 is considered, then the flux balance of ions will be satisfied, but Eq. 84 may not be satisfied and lead to a charge gradient prediction. If Eq. 84 of electroneutrality is enforced, the flux balance may not then be satisfied. Hence, from mathematical considerations, one may solve the anomaly by using the same value of diffusivity for all the ions, and, hence, be consistent in satisfying the flux balance, as well as the condition of electroneutrality

$$D^L_{NO_2^-}(\text{new}) = D^L_{NO_3^-}(\text{new}) = D^L_{OH^-}(\text{new}) = D^L_{H^+}(\text{new}) = D_{\text{eff}} \quad (85)$$

The effective diffusivity is thus the resultant diffusivity. Its physical significance is that the faster ion is retarded, and the slower ions' movement is accelerated by virtue of the electric forces in a solution containing various ionic species (Brogren and Karlsson, 1997). Although there can be more rigorous treatment of this part using Nernst Planck equations, the above approach has been adopted for simplicity. Equation 82 can be elaborated as

$$Z + Y[B^{Y+}(aq)] - \frac{K_{37}}{Z} - K_{36}\frac{W}{Z} - [NO_3^-(aq)] = 0 \quad (86)$$

$$Z^2 + \{Y[B^{Y+}(aq)] - [NO_3^-(aq)]\}Z - K_{37} - K_{36}W = 0 \quad (87)$$

Thus

$$Z^2 + D_2 Z - F_2 - E_2 W = 0 \quad (88)$$

where $D_2 = \{Y[B^{Y+}(aq)] - [NO_3^-(aq)]\}$, $F_2 = K_{37}$, $E_2 = K_{36}$. Substituting from Eq. 78

$$Z^2 + D_2 Z - F_2 - E_2\left(\frac{-A_2 Z}{B_2 Z + C_2}\right) = 0 \quad (89)$$

$$B_2 Z^3 + (D_2 B_2 + C_2)Z^2 + (C_2 D_2 - B_2 F_2 + E_2 A_2)Z - C_2 F_2 = 0 \quad (90)$$

$$Z^3 + \frac{(D_2 B_2 + C_2)}{B_2}Z^2 + \frac{(C_2 D_2 - B_2 F_2 + E_2 A_2)}{B_2}Z - \frac{C_2 F_2}{B_2} = 0 \quad (91)$$

This is a cubic equation in Z. From its solution, $Z = [H^+(aq)]$ at $x = \Delta x_L$ is obtained. The other concentrations of HNO_2, OH^-, NO_2^- are calculated from Eqs. 78, 72, and 73. Corresponding fluxes ψ_I are obtained from Eq. 60.

The various values of model parameters (rate constants, equilibrium constants, Henry's constants, diffusivities), which were used in the model, are given in Table 5.

Method of numerical solution

There are eight coupled, second-order differential equations (Eqs. 29–36) for the gas film and a set of 11, coupled second-order differential equations (Eqs. 37–47) describing the mass transfer with chemical reactions in the liquid film. A single second-order differential equation needs two boundary conditions for solution. The present gas liquid absorption

Table 5. Model Parameters

Model Parameter and Reference		Values
Gas-phase diffusivity D_I^G, $T = 298$K,	NO	2.3×10^{-5} m^2/s
$P = 1.013\times10^5$ N/m^2 (Newman and Carta, 1988)	NO_2	1.4×10^{-5}
	N_2O_3	1.1×10^{-5}
$D_J^G(T_2,P_2) = D_J^G(T_1,P_1)\left(\frac{T_2}{T_1}\right)^{1.75}\left(\frac{P_1}{P_2}\right)$	N_2O_4	0.98×10^{-5}
	O_2	1.5×10^{-5}
	H_2O	2.6×10^{-5}
	HNO_2	1.4×10^{-5}
	HNO_3	$\sim 1.4\times10^{-5}$
Liquid-phase diffusivity D_I^L at $T = 298$ K	NO	1.45×10^{-9} m^2/s
(Shadid and Handley, 1990)	NO_2	1.45×10^{-9}
$\frac{D_J^L\mu_L}{T} = $ constant	N_2O_3	1.4×10^{-9}
	N_2O_4	1.4×10^{-9}
	O_2	1.5×10^{-9}
	HNO_2	1.8×10^{-9}
	H^+	4.0×10^{-9}
	OH^-	3.7×10^{-9}
	Ca^{++}	1.5×10^{-9}
	NO_2^-	2.8×10^{-9}
	NO_3^-	2.8×10^{-9}
		Effective diffusivity of ions, $D_{\text{eff}} = 2.914\times10^{-9}$
Solubility	NO	1.84×10^{-8} kmol/m^3(N/m^2)
Henry's Constant $T = 298$ K	NO_2	1.18×10^{-7}
(Schwartz and White, 1981)	N_2O_3	5.92×10^{-6}
	N_2O_4	1.38×10^{-5}
	HNO_2	4.8×10^{-4}
	O_2	1.1×10^{-8}
K_{42}	HNO_3	32.18 (k-ion/m^3)^2/(N/m^2)
Equilibrium constants	K_2	$K_2 = 10^{(2993/T - 9.226)}\times1.013\times10^5$/RT (m^3/kmol)
(Suchak, 1989; Schwartz and White, 1981;	K_3	$K_3 = 10^{(2072/T - 7.234)}\times1.013\times10^5$/RT (m^3/kmol)
England and Corcoran, 1975);	K_4	$K_4 = 10^{(-20.83/T - 0.5012)}$
	K_5	$K_5 = 10^{(-965.5/T - 1.481)}$
	K_{32}	6.54×10^4 m^3/kmol at 298 K
	K_{33}	1.37×10^4 m^3/kmol at 298 K
	K_{34}	330 at 298 K
	K_{35}	5.81×10^4 at 298 K
	K_{36}	5.1×10^{-4} at 298 K
	K_{37}	1×10^{-14} at 298 K
Rate constants	k_1	$k_1 = (10^{652.1/T - 0.7356})\left[\frac{RT}{1.013\times10^5}\right]^2$
(Pradhan and Joshi, 1999; Newman and Carta, 1988;		(m^3/kmol)^2/s
Schwartz and White, 1981; England and Corcoran, 1975)	k_{4F}	$k_{4F} = 4.1\times10^4$ m^3/kmol/s
	k_{4B}	$k_{4B} = k_{4F}/K_4$
	k_{5F}	$k_{5F} = 2.5\times10^2$ m^3/kmol/s
	k_{5B}	$k_{5B} = k_{5F}/K_5$
	k_{33F}	1.37×10^6 m^3/kmol/s
	k_{33B}	k_{33F}/K_{33}
	k_{32F}	$k_{32F} \cong k_{33F}$
	k_{32B}	$k_{32B} = k_{32F}/K_{32}$
	k_{34F}	8.68×10^5 L/s
	k_{34B}	$k_{34B} = k_{34F}/K_{34}$
	k_{35F}	157.2 L/s
	k_{35B}	$k_{35B} = k_{35F}/K_{35}$

is a *boundary value problem* in which the concentrations of the components are known at the boundary viz. gas bulk ($x_G = 0$) and liquid bulk ($x_L = \delta_L$). In addition, there is a separate equation to describe the (diffusion + reaction) of a component I in the gas film and the liquid film. Hence, it was required to have connecting equations of concentration of component I, $[I(\mathrm{g})]$ at $x_G = \delta_G$ and $[I(aq)]$ at $x_L = 0$, that is, at the gas liquid interface. Similarly, the fluxes of the components needed to be connected at the gas/liquid interface. Besides the diffusion equations, the constraints of equilibria along the gas/liquid film are accommodated by the method of Oleander (1960), as shown in Appendix A.

The boundary value problem can be solved by the *Shooting Method* (Press et al., 1998). It involves guessing the concentration gradients at one boundary. Knowing the specified concentration and guess gradients at this boundary (gas bulk), the differential equations are discretized and integrated by marching the solution up to the other boundary (liquid bulk). The calculated values of concentrations are compared with the desired values of the concentration of the other boundary. The solution is converged by the Newton Raphson method. The fluxes of the various components leaving the gas bulk (entering the gas film) and the components entering the liquid bulk (leaving from the liquid film) can be calculated. Thus, the point rates of NO_X removal are obtained. Although there is mass transfer of all the NO_X species, the term "NO_X removal rate" used here particularly pertains to the flux of $(\psi_{NO_2^-} + \psi_{NO_3^-} + \psi_{HNO_2})|x_L = \delta_L$ leaving the liquid film and entering the liquid bulk. The selectivity (η) of nitrite is defined by

$$\eta = \frac{\left(\psi_{NO_2^-} + \psi_{HNO_2}\right)}{\left(\psi_{NO_2^-} + \psi_{NO_3^-} + \psi_{HNO_2}\right)}|x_L = \delta_L \qquad (92)$$

Since the quantities such as gas and liquid side concentrations of the components, as well as the various rates of reaction, vary over several orders of magnitude, all the concentration and distance terms were nondimensionalized with respect to the suitable quantities such as bulk concentration, film thickness, and so on. The problem was converted into dimensionless form, followed by numerical solution.

Results and Discussion

Reconstruction of events during the mass-transfer process

When a NO_X laden gas is contacted with a liquid, mass transfer of the species NO, NO_2, N_2O_3, N_2O_4, HNO_2, HNO_3 occurs. The direction depends on the driving force. During diffusion, the reactions take place simultaneously in the liquid phase (Figure 1). After it enters the liquid film, N_2O_3 undergoes hydrolysis to give HNO_2, whereas N_2O_4 gives HNO_2 and HNO_3. The absorbed HNO_2, as well as HNO_2 which is formed in the liquid phase, can remain in the dissociated or undissociated state. The HNO_3 absorbed into/formed in the liquid phase is considered to be practically present only in the dissociated form as H^+ and NO_3^-.

The reverse of the N_2O_3/N_2O_4 hydrolysis reactions can also occur. As N_2O_3/N_2O_4 proceeds from the interface towards the liquid bulk, it may get exhausted since the forward reaction is fast and the rate of reverse reaction may be small. However, their reaction products (HNO_2, H^+, NO_3^-) continue to travel on further in the liquid film. If the liquid bulk is acidic, the HNO_2 can extend right up to the liquid bulk and exist in the liquid bulk too.

However, if the liquid phase is slightly alkaline, the HNO_2 and H^+ species diffusing from the interface towards the liquid bulk encounter the OH^- ions diffusing from the liquid bulk side toward the interface. They neutralize each other at a "reaction front" located at, say, a distance λ from the interface. Thus, λ is located in the liquid film $0 \le (\lambda/\delta) \le 1$. A value of $(\lambda/\delta) = 1$ means that the HNO_2 has reached the liquid bulk and the entire film is acidic.

If the liquid bulk is alkaline, the value of (λ/δ) may be less than 1. Thus, it may be considered that there is enhancement in the mass transfer rate of OH^-, due to chemical reaction and these ions have to diffuse a shorter distance (δ-λ). Since the OH^- ions predominate over the H^+ ions in the alkaline region of the film ($\lambda < x_L < \delta$), concentration of HNO_2 in this region is practically zero. Thus, the decomposition of HNO_2 to N_2O_3, and further to NO and NO_2, is restricted only to the region ($0 < x_L < \lambda$). Hence, there is an increase in the rate of NO_X removal in terms of HNO_2, NO_2^- fluxes entering the liquid bulk. This is due to: (a) lesser scope for decomposition of HNO_2, and (b) a smaller diffusion path leading to enhancement compared to the case of NO_X absorption in acid. Selectivity of NO_2^- over NO_3^- is also increased. When the liquid is made further alkaline, then the OH^- ions may pervade right up to the interface itself. Practically no free HNO_2 can then exist in the liquid phase, because the OH^- ions instantaneously neutralize the HNO_2 absorbed, as well as that formed from hydrolysis. The rate of NO_X removal is high, as well as the selectivity is high. Any further increase in the bulk OH^- ion concentration is not expected to provide further enhancement in the rate of NO_X removal or selectivity, because all the possible HNO_2 decomposition has already been curbed.

One can now compare the predictions of the model with the visualized process (Figures 2 to 7). The model was solved numerically for the case of gas with NO_X content $= 1.5\%$ mol, NO/NO_2 ratio of 10, $T = 328$ K, $P = 1.013 \times 10^5$ N/m^2, $k_G = 0.5$ m/s, $k_L = 2 \times 10^{-4}$ m/s. Figure 2A shows how the location of $(\%\ \lambda/\delta)$ varies with an increase in the OH^- concentration of liquid bulk, whereas Figure 2B shows the same except that the x axis has a linear scale. In the acidic range ($[OH^-]^B < 10^{-7}$ k-ion/m^3), the $(\%\ \lambda/\delta) = 100$. As the alkalinity of the solution increases, the location of the reaction front moves inward towards the interface, due to diffusion of the OH^- ions into the liquid film. At a certain $[OH^-]^B$ concentration of ~ 0.05 k-ion/m^3, the $(\%\ \lambda/\delta) = 0$, that is, the OH^- ion pervades right up to the interface.

Figures 3A and 3B show how the selectivity η of nitrite over nitrate varies, with change in OH^- concentration. As the bulk OH^- concentration increases from the mildly acidic to alkaline range, the selectivity increases as long as $(\%\ \lambda/\delta) > 0$. When the $[OH^-]^B$ is increased further, the interface becomes more alkaline and there is no further enhancement in selectivity. A similar trend is seen with the rate of NO_X removal, as shown in Figures 4A and 4B.

Figures 5A and 5B show how the interfacial OH^- concentration $[OH^-]^*$ changes with the bulk concentration of OH^-. When the liquid bulk is acidic, the interface is more acidic

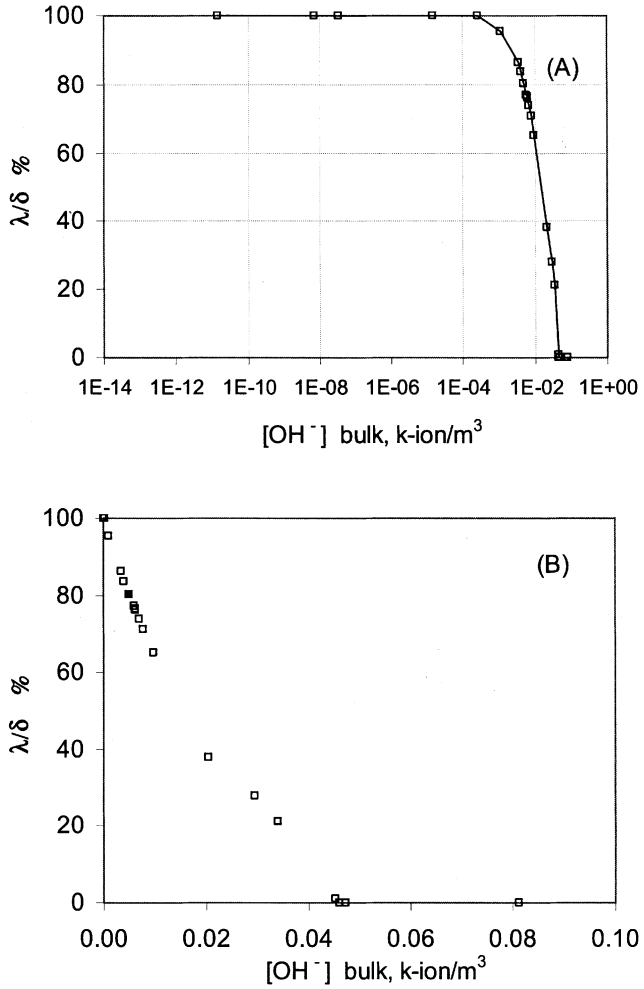

Figure 2. Variation of location of the reaction front with $[OH^-]^B$ (A and B).

Total $NO_X = 1.5\%$mol, $NO^*/NO_2^* = 10$, $T = 328$ K, $P = 1.013\times10^5$ N/m^2, $k_G = 0.5$ m/s, $k_L = 2\times10^{-4}$ m/s.

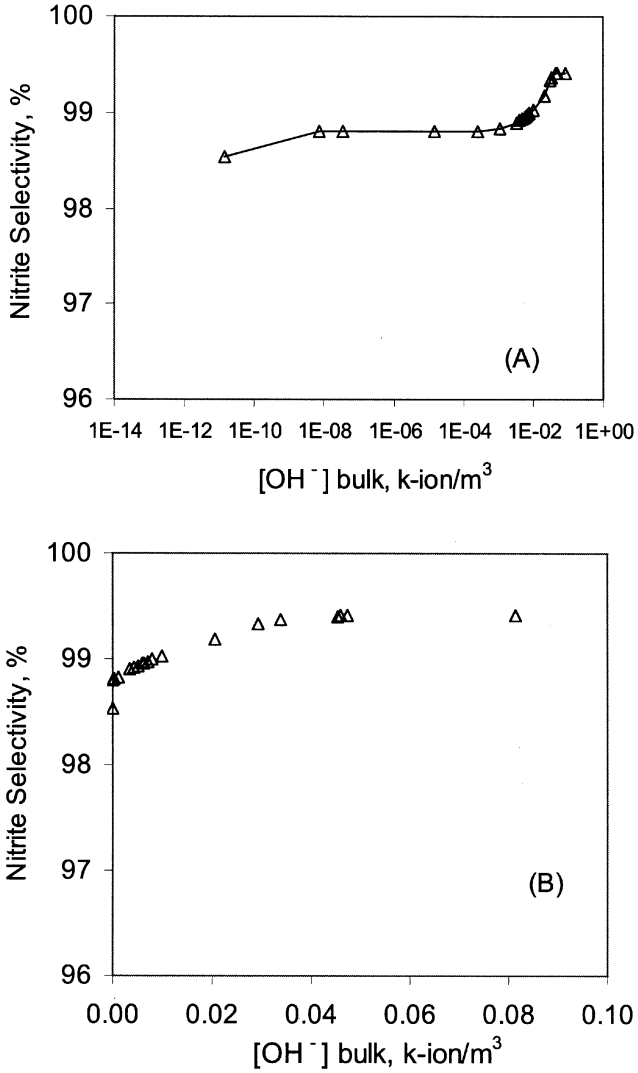

Figure 3. Variation of the nitrite selectivity with $[OH^-]^B$ (A and B).

Total $NO_X = 1.5\%$mol, $NO^*/NO_2^* = 10$, $T = 328$ K, $P = 1.013\times10^5$ N/m^2, $k_G = 0.5$ m/s, $k_L = 2\times10^{-4}$ m/s.

during absorption. When the liquid bulk is made mildly alkaline, the interface has lower acidity. Above a certain bulk $[OH^-]$ concentration, [higher than for $(\%\ \lambda/\delta) > 0$], the interfacial alkalinity increases such that $[OH^-]^B - [OH^-]^* =$ constant, as seen from Figure 6. This represents a constant consumption of OH^- ions viz. $\{k_L([OH^-]^B - [OH^-]^*\}$, which complements the leveled off NO_X removal rate. Figure 7 shows how the dimensionless gas side concentration gradient of HNO_2

$$\left[\frac{d[HNO_2(g)]/[HNO_2(g)]^B}{d(x_G/\delta_G)}\right]_{x_G=0}$$

varies the location of the reaction front $\%(\lambda/\delta)$. As the liquid phase is more and more alkaline, there is a steeper gradient of HNO_2 and finally the slope remains -1 at high alkalinity.

Contribution of various components

The NO_X gases in a mixture exist in equilibrium. The NO_X components react among each other to attain a certain composition of the various components (NO, NO_2, N_2O_3, N_2O_4, HNO_2, HNO_3). This composition depends on the total NO_X content, ratio of divalent to tetravalent NO_X in the mixture, temperature, pressure, and moisture content.

Typically, at low partial pressure of NO_X, the NO and NO_2 may be present in greater proportions among the NO_X components, but they have poor solubility; so, their rate of absorption is *low*. The N_2O_3/N_2O_4 may be present in lower proportions, but they have higher solubility compared to NO/NO_2; hence, their rate of absorption is *high*. The HNO_2 and HNO_3 are present in still lower proportions in the gas phase, but they have very high solubilities and their contribution to the rate of NO_X removal can be *high/moderate*. Thus, the combined effect of solubility and gas-phase partial pres-

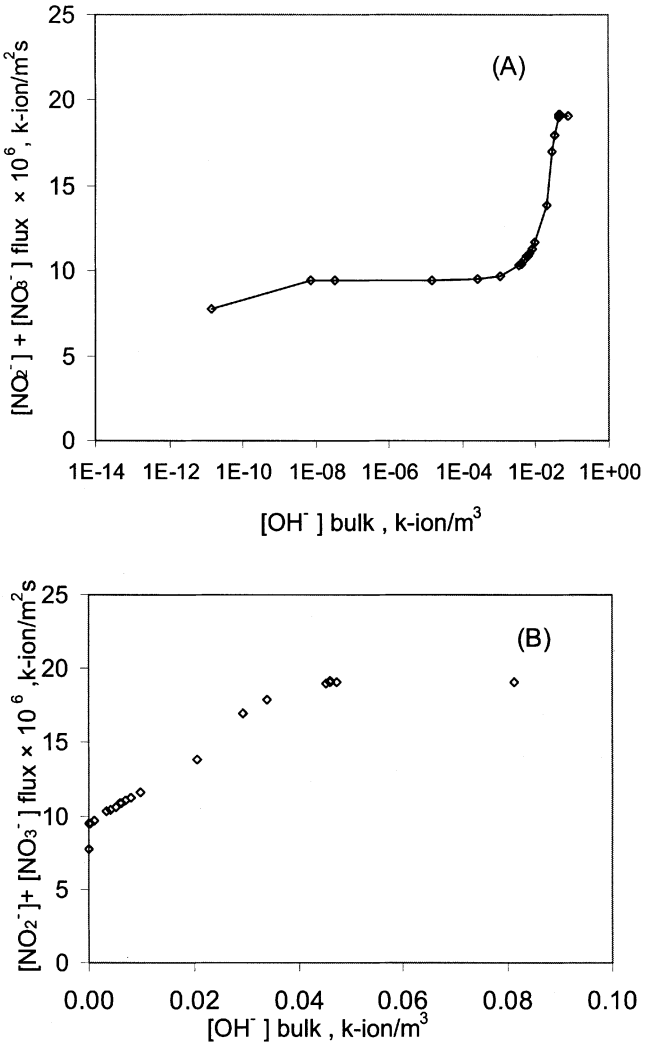

Figure 4. Variation of the NO_X removal rate with $[OH^-]^B$ (A and B).

Total $NO_X = 1.5\%$mol, $NO^*/NO_2^* = 10$, $T = 328$ K, $P = 1.013\times10^5$ N/m^2, $k_G = 0.5$ m/s, $k_L = 2\times10^{-4}$ m/s.

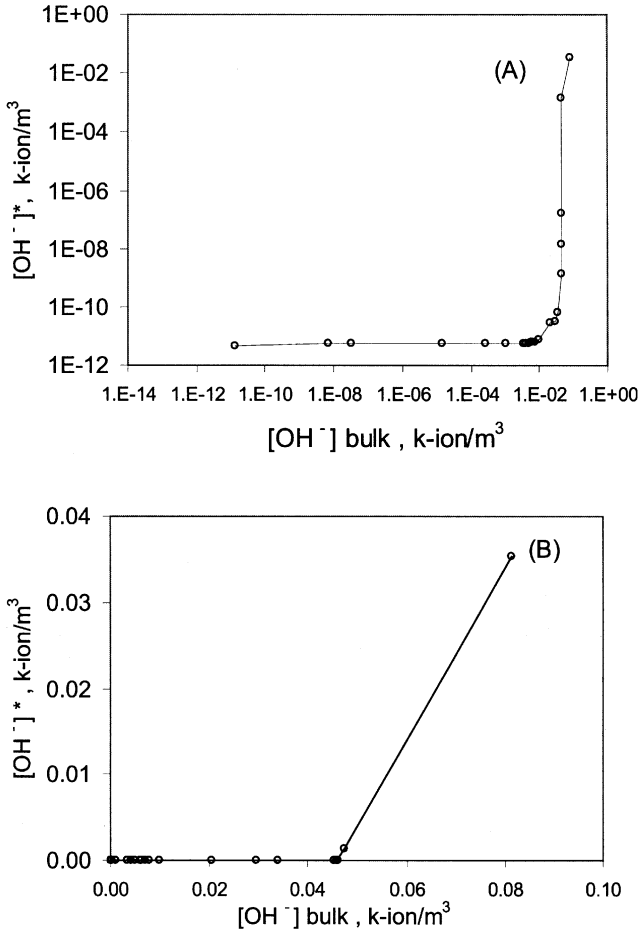

Figure 5. Variation $[OH^-]^*$ with $[OH^-]^B$ (A and B).

Total $NO_X = 1.5\%$mol, $NO^*/NO_2^* = 10$, $T = 328$ K, $P = 1.013\times10^5$ N/m^2, $k_G = 0.5$ m/s, $k_L = 2\times10^{-4}$ m/s.

sure can affect the rate of absorption of each component. Moreover, the rate of mass transfer is enhanced by the liquid-phase hydrolysis of N_2O_3 and N_2O_4 and the neutralization of HNO_2 and HNO_3 by OH^-.

In the gas film, the hydrolysis of N_2O_3 to HNO_2 is favored by the presence of water, and is advantageous as HNO_2 has higher solubility than N_2O_3, and rates are improved. The gas-phase reaction of N_2O_4 with water is slow and contributes only slightly to HNO_2/HNO_3 formation.

Effect of various parameters

The model predictions matched with the qualitative expectations which arose from the visualization of this absorption and reaction process. Next, the sensitivity of NO_X removal rate and selectivity to the changes in various parameters was quantified. These simulation results are discussed here. The effects of parameters were studied such as total NO_X content in the gas phase, NO^*/NO_2^* ratio, temperature, pres-

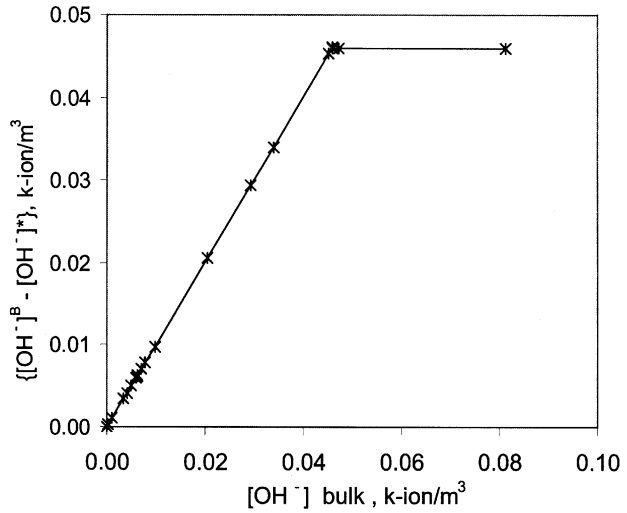

Figure 6. Extent of $[OH^-]$ depletion in the liquid film.

Total $NO_X = 1.5\%$mol, $NO^*/NO_2^* = 10$, $T = 328$ K, $P = 1.013\times10^5$ N/m^2, $k_G = 0.5$ m/s, $k_L = 2\times10^{-4}$ m/s.

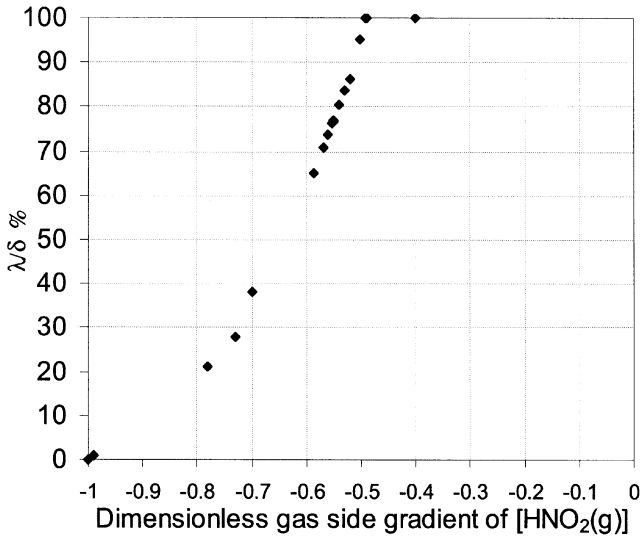

Figure 7. Relation between reaction front location and dimensionless [HNO_2(g)] gradient.

Total $NO_X = 1.5\%$mol, $NO^*/NO_2^* = 10$, $T = 328$ K, $P = 1.013\times10^5$ N/m^2, $k_G = 0.5$ m/s, $k_L = 2\times10^{-4}$ m/s.

sure, and water content in the gas phase k_G, k_L. The liquid composition was varied over a wide range of pH, as shown in Table 6, at constant secondary cation concentration $[M^{Y+}]$.

Effect of Total NO_X Composition. The model simulated the absorption for the case of gas with three different NO_X content (1,000 ppm, 10^4 ppm, 10^5 ppm) over a wide range of liquid bulk $[OH^-]$ concentration. ($T = 328$ K, $P = 1.013\times10^5$ N/m^2, $k_G = 0.05$ m/s, $k_L = 1\times10^{-4}$ m/s, $NO^*/NO_2^* = 10$, $[Ca^{++}]^* = 0.5$ k-ion/m^3). As expected, when the NO_X content of the gas increases, the rate of NO_X removal increases (Figure 8a). Since the internal composition of the equilibrium mixture of NO_X gases changed only slightly with the change in total NO_X content, there is only a slight increase in the selectivity with the increase in the total NO_X content (Figure 8b).

Effect of NO^*/NO_2^* Ratio of the Bulk Gas. The (NO^*/NO_2^*) ratio was varied over a logarithmic range (0.1, 1, 10) with total $NO_X = 1{,}000$ ppm, $T = 328$ K, $P = 1.013\times10^5$ N/m^2, $k_G = 0.05$ m/s, $k_L = 1\times10^{-4}$ m/s, $[Ca^{++}]^* = 0.5$ k-ion/m^3. As the NO^*/NO_2^* ratio is increased, the concentration of NO_2 decreases in the gas-phase equilibrium mixture,

Table 6. Liquid-Phase Ionic Composition

	$[OH^-]^B$ k-ion/m^3	$[H^+]^B$ k-ion/m^3	$Y[M^{Y+}]^B$ k-ion/m^3	$[NO_2^-]^B$ k-ion/m^3	$[NO_3^-]^B$ k-ion/m^3
pH					
3	10^{-11}	10^{-3}	1.0	1.00090	0.0001
5	10^{-9}	10^{-5}	1.0	0.99991	0.0001
7	10^{-7}	10^{-7}	1.0	0.99990	0.0001
9	10^{-5}	10^{-9}	1.0	0.99989	0.0001
11	10^{-3}	10^{-11}	1.0	0.99890	0.0001
12	10^{-2}	10^{-12}	1.0	0.98990	0.0001
13	10^{-1}	10^{-13}	1.0	0.89990	0.0001
14	1	10^{-14}	1.02	0.01990	0.0001

{M^{Y+} = secondary cation, such as Na^+/K^+ ($Y = 1$); Ca^{2+}/Mg^{2+} ($Y = 2$)}.

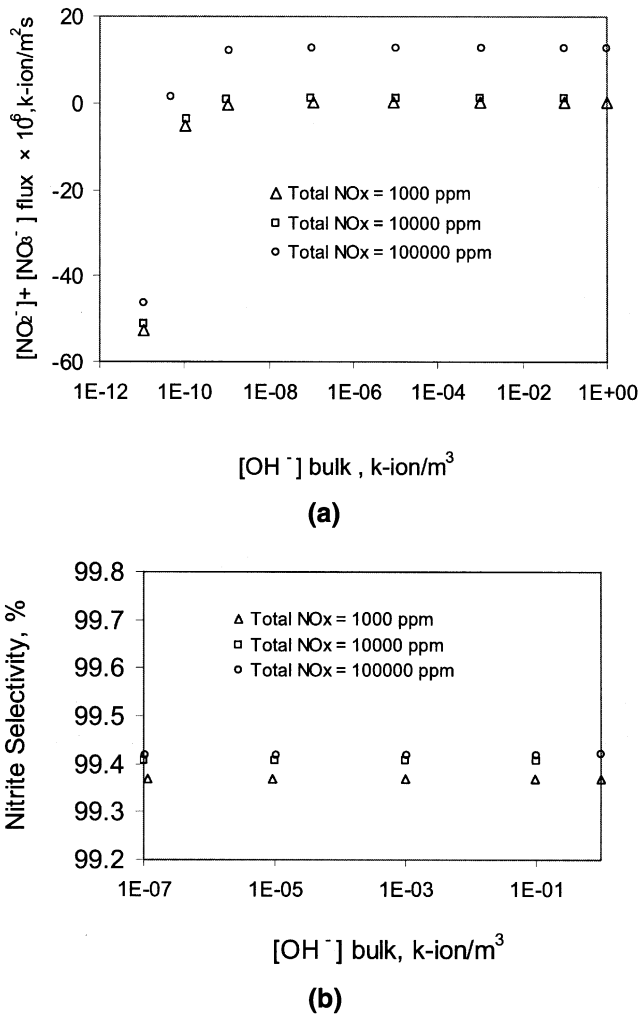

Figure 8. Effect of total NO_X content on (A) the NO_X removal rate (B) selectivity.

$NO^*/NO_2^* = 10$, $T = 328$ K, $P = 1.013\times10^5$ N/m^2, $k_G = 0.05$ m/s, $k_L = 1\times10^{-4}$ m/s.

which reduces the equilibrium content of N_2O_4 and HNO_3. There is also a decrease (to a smaller extent) in the N_2O_3 and HNO_2 concentrations. Hence, the overall effect is that, as the NO^*/NO_2^* ratio increases, the selectivity increases (Figure 9B). However, the rate of NO_X removal decreases, due to lesser bulk concentrations of N_2O_4, N_2O_3, HNO_2, HNO_3 (Figure 9A).

Effect of Temperature. Figures 10A and 10B show the effect of temperature on the NO_X removal rate and selectivity (total $NO_X = 1{,}000$ ppm, $NO^*/NO_2^* = 10$, $P = 1.013\times10^5$ N/m^2, $k_G = 0.05$ m/s, $k_L = 1\times10^{-4}$ m/s, $[Ca^{++}]^* = 0.5$ k-ion/m^3). At each temperature, the gas phase was considered almost saturated with water vapor. As the temperature increases from 298 K to 328 K, there is improvement in the rate of NO_X removal and selectivity, however, from 328 K to 343 K, the selectivity is hardly affected, whereas the NO_X removal rate goes down very slightly. As the temperature is increased, the water content in the gas phase is more at saturation condition. This aids the formation of HNO_2 from NO, NO_2, and H_2O. Hence, the HNO_2 content in the gas phase

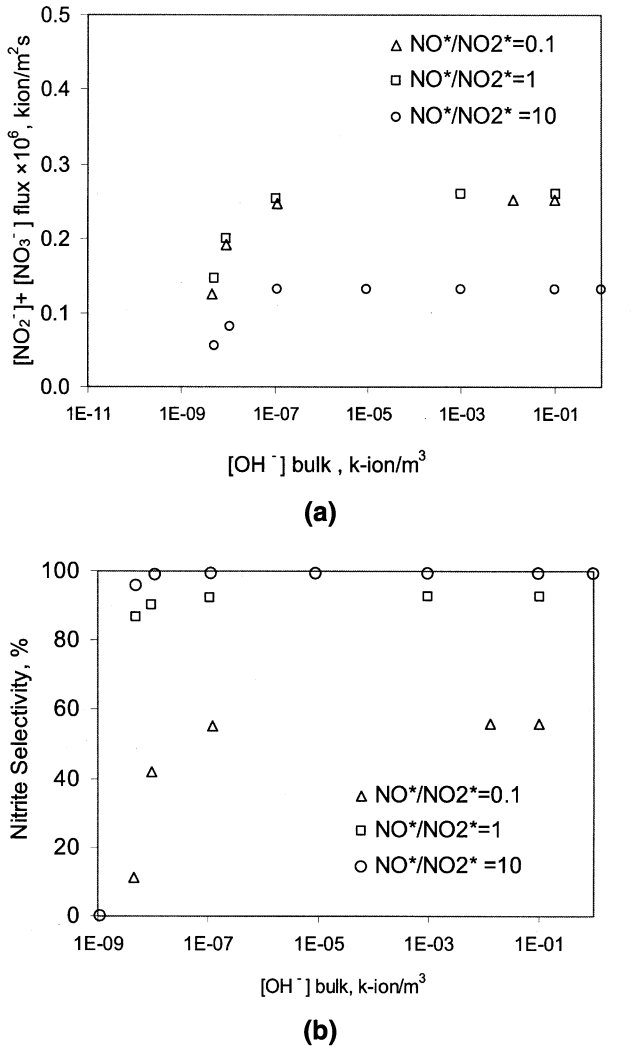

Figure 9. Effect of NO^*/NO_2^* content on (A) the NO_X removal rate (B) selectivity.

Total $NO_X = 1{,}000$ ppm, $T = 328$ K, $P = 1.013 \times 10^5$ N/m^2, $k_G = 0.05$ m/s, $k_L = 1 \times 10^{-4}$ m/s.

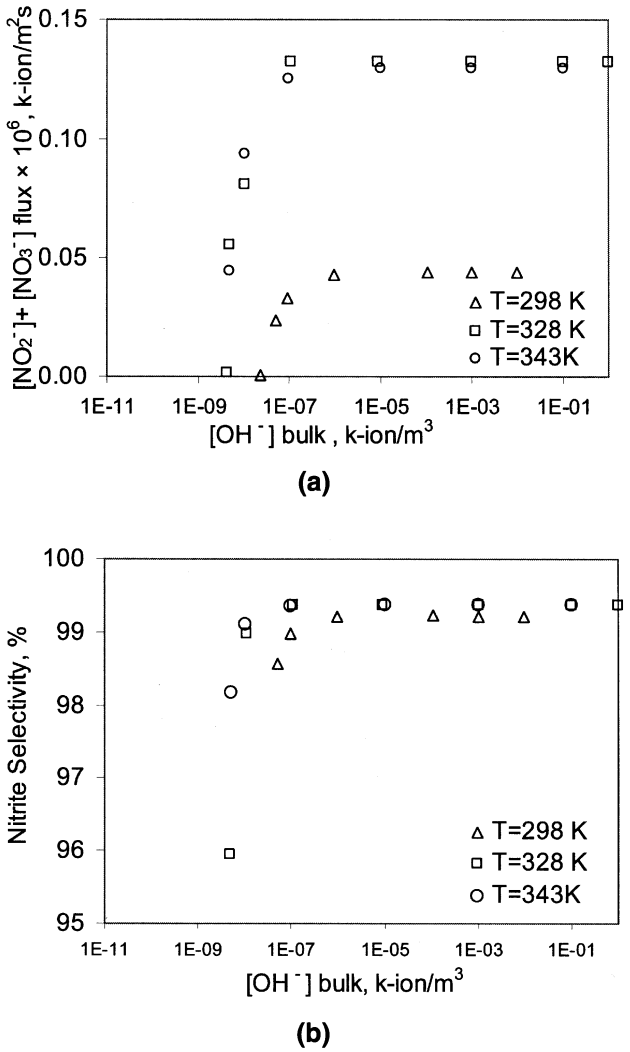

Figure 10. Effect of temperature on (A) the NO_X removal rate (B) selectivity; at various $[OH^-]^B$ concentration.

Total $NO_X = 1{,}000$ ppm, $NO^*/NO_2^* = 10$, $P = 1.013 \times 10^5$ N/m^2, $k_G = 0.05$ m/s, $k_L = 1 \times 10^{-4}$ m/s.

increases and the NO_X removal rate is higher. However, with the rise in the temperature, the equilibrium constant of the reaction described in Eq. 6 falls rapidly. The equilibrium constant of reaction in Eq. 8 is less sensitive to temperature. The net result is a fall in the equilibrium HNO_2 concentration, which lowers the NO_X removal rate (Figures 11A and 11B).

Effect of Pressure. The total pressure does not seem to have much effect on the selectivity (Figure 12B), because the internal composition of the NO_X components does not vary much with the total pressure. However, with the increase in the total pressure, the rate of NO_X removal increases (Figure 12A), since the driving force for mass transfer increases.

Effect of Gas Side Mass-Transfer Coefficient. Figures 13A and 13B show the rate of NO_X removal and selectivity at two values of k_G (0.05 m/s, 0.5 m/s). A high value of k_G increases the rate of NO_X removal, which can be understood in terms of a shorter diffusion path length for each diffusing molecule, that is, lower resistance.

Each one of the absorbed species such as NO_2, N_2O_3, N_2O_4, HNO_2, HNO_3 can contribute to the total rate of NO_X removal and overall nitrite selectivity. When the gas film resistance is low (that is, the value of k_G is high), then, in spite of poor solubility, some significant NO_2 is also absorbed, which contributes to nitrite, as well as nitrate formation. The formation of nitrate reduces the nitrite selectivity.

However, when the gas film resistance is large (that is, value of k_G is low) in addition to the poor solubility of NO_2, the rate of NO_2 transfer is low. The formation of nitrate is lower. The variation in the gas-phase partial pressures of the NO_X components, the diffusivities, and solubilities leads to differential/preferential formation of nitrites and nitrates. By virtue of the widely varying solubilities of the various components in the liquid phase, the interface acts as a "filter," selectively absorbing more of the soluble components. Similarly, the gas side resistance also plays a role in determining selectivity. A lower k_G offers greater "filtering" action and results in higher selectivity of NO_2^-. (See Appendix B.)

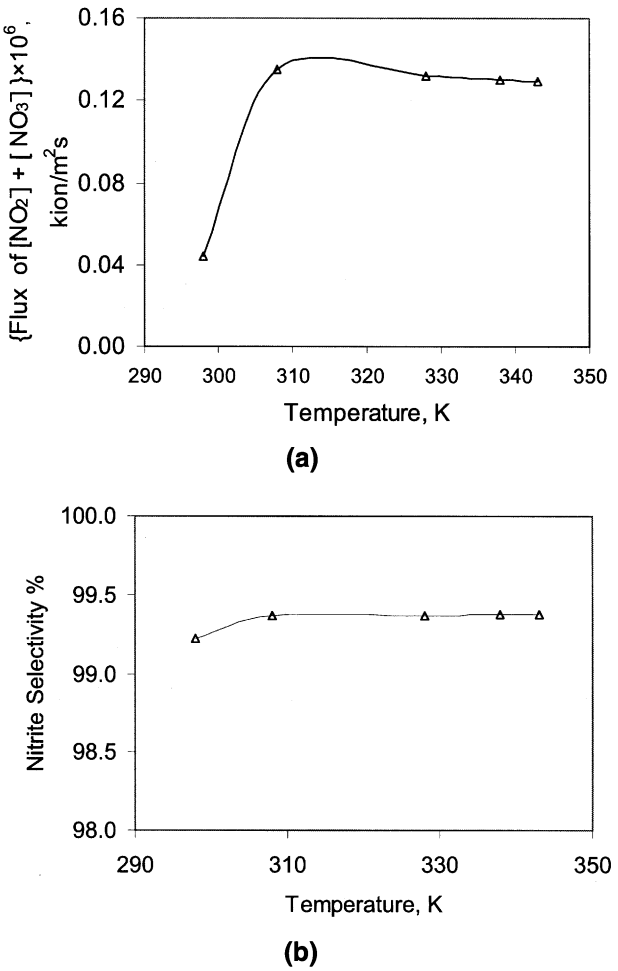

Figure 11. Effect of temperature on (A) the NO_X removal rate (B) selectivity.

Total $NO_X = 1{,}000$ ppm, $P = 1.013 \times 10^5$ N/m^2, $k_G = 0.05$ m/s, $k_L = 1 \times 10^{-4}$ m/s, $[OH^-]^B = 0.001$ k-ion/m^3.

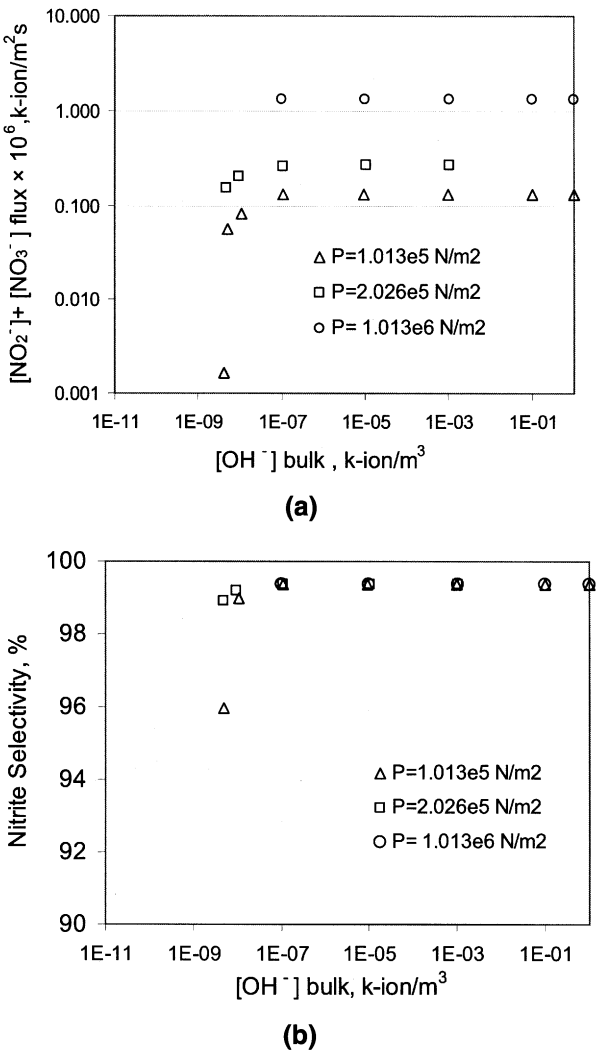

Figure 12. Effect of pressure on (A) the NO_X removal rate (B) selectivity.

Total $NO_X = 1{,}000$ ppm, $NO^*/NO_2^* = 10$, $T = 328$ K, $k_G = 0.05$ m/s, $k_L = 1 \times 10^{-4}$ m/s.

Effect of the Liquid Side Mass-Transfer Coefficient. The value of k_L was varied over a range from 10^{-5} m/s to 2×10^{-4} m/s for the case of total $NO_X = 1{,}000$ ppm, $NO^*/NO_2^* = 10$, $T = 328$ K, $P = 1.013 \times 10^5$ N/m^2, $k_G = 0.05$ m/s, $[OH^-]^B = 0.001$ m/s. There was practically no effect of k_L on the rate of NO_X removal and selectivity. This is so because, in the case of absorption of low concentration of NO_X in alkaline solution, the liquid-phase hydrolysis of N_2O_3 and N_2O_4 almost undergoes completion within a very short distance, which is much lesser than the liquid film thickness. Hence, increasing the liquid film thickness (thereby lowering k_L) does not affect the absorption rate. In alkaline solution, the HNO_2 decomposition is minimal. Hence, the selectivity is also not much affected by k_L, as long as $\lambda > 0$.

Effect of Water Vapor Content of the Gas. The effect of water vapor in the gas phase was also studied, although practically, the vapor phase can get saturated rapidly on contact with the aqueous phase. (See Figures 14A and 14B.) When the gas phase is unsaturated with respect to water, the rate of NO_X removal and selectivity are lower. This is so due to the correspondingly lower HNO_2 concentrations in the gas phase.

Effect of the $[M^+]$ Cation Concentration. There is electroneutrality at all points along the length of the liquid film and at the interface too. The cations are $[H^+]$ and the other cation (if any) such as $[Ca^{++}]$, $[Na^+]$, $[NH_4]^+$. The anions are $[OH^-]$, $[NO_2^-]$ and $[NO_3^-]$. The model formulation of the equilibrium at the gas liquid interface shows that the cation concentration is also involved in the aqueous ionic equilibria at the interface. When the salts are present in the solution, the concentrations of cations and anions increase. For the case of total $NO_X = 1{,}000$ ppm, $NO^*/NO_2^* = 10$, $k_G = 0.05$ m/s, $k_L = 10^{-4}$ m/s, $T = 328$ K, $P = 1.013 \times 10^5$ N/m^2, and the liquid side cation concentration $[M^{++}(aq)]^B$ was changed from 0, 0.5, and 3 k-ion/m^3. For electroneutrality, the additional counter-ions of $[NO_2^-(aq)]^B$ were specified. The $[H^+(aq)]^B$ and $[OH^-(aq)]^B$ were specified at 10^{-7}, neutral conditions. The increase in the metal cation concentration lowers the rate of NO_X removal, as well as the selectivity. (See Figures 15A and 15B.)

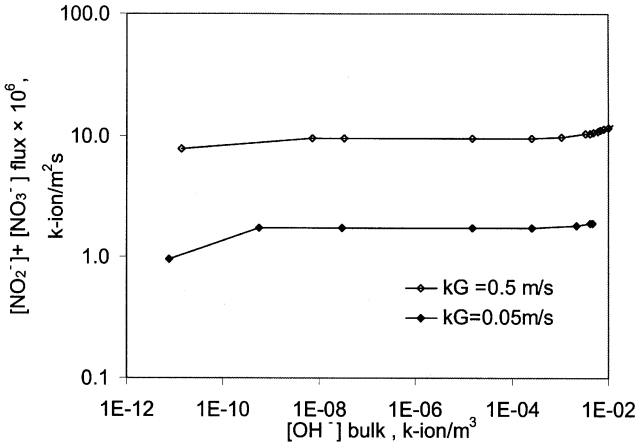

(a)

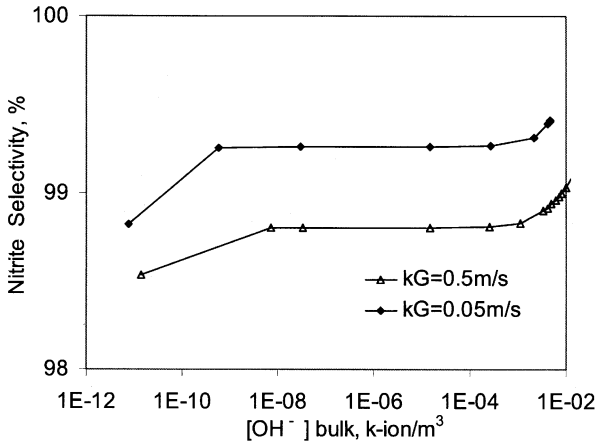

(b)

Figure 13. Effect of gas side mass-transfer coefficient (A) the NO_X removal rate (B) selectivity.

Total $NO_X = 1{,}000$ ppm, $NO^*/NO_2^* = 10$, $T = 328$ K, $P = 1.013 \times 10^5$ N/m^2, $k_L = 1 \times 10^{-4}$ m/s.

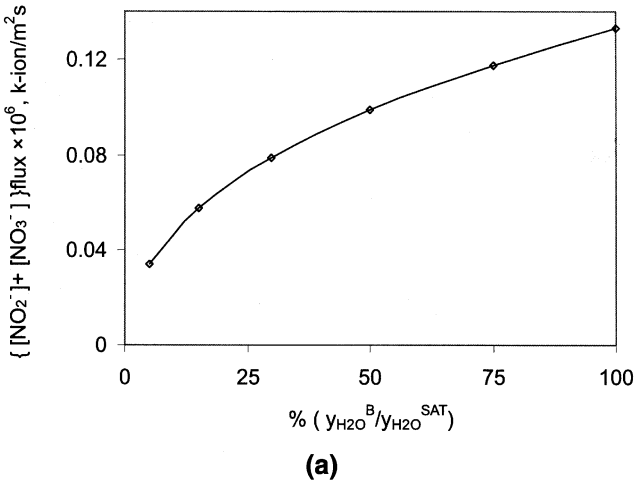

(a)

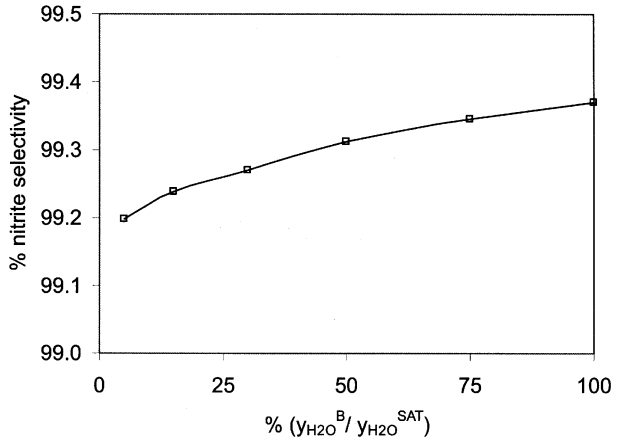

(b)

Figure 14. Effect of moisture content in the bulk gas, on (A) the NO_X removal rate (B) selectivity.

Total $NO_X = 1{,}000$ ppm, $NO^*/NO_2^* = 10$, $T = 328$ K, $P = 1.013 \times 10^5$ N/m^2, $k_G = 0.05$ m/s, $k_L = 1 \times 10^{-4}$ m/s.

When there is a finite partial pressure of HNO_2 at the interface, it has a corresponding saturation concentration $[HNO_2(aq)]^*$ in the liquid phase. $[HNO_2(aq)]$ is in equilibrium with $[H^+(aq)]^*$ and $[NO_2^-(aq)]^*$. An increase in the $[NO_2^-(aq)]^B$ leads to a reduction in the overall driving force and, hence, the selectivity and rate are lower. Moreover, the increase in the solution viscosity also affects the diffusivity and rates.

Model comparison with $Ca(NO_2)_2$ patent data

In this section, the rate of NO_X removal and selectivity inferred from a patented calcium nitrite process have been compared with the model predictions. The comparison will be summarized in Table 8.

High purity calcium nitrite has a market value as corrosion inhibitor, reactive intermediate, antifreeze agent, and so on. It can be produced by NO_X absorption in $Ca(OH)_2$. Literature on $Ca(NO_2)_2$ process/purification is scant. Most of it is in the form of patents (Takakuwa and Arima, 1975; Takakuwa et al., 1976; Endo and Kushahara, 1980; Gaidis and Rosenberg, 1981; Bean et al., 1981; Peretrutov et al., 1982; Zhantalai et al., 1985). In the few commercial processes producing $Ca(NO_2)_2$ of capacity ca. 7,000 TPA, the NO_X gases are deliberately produced by ammonia oxidation, but there is also a possibility to use polluting NO_X gases (arising from some process). In this way, the problem of pollution control can be converted to a profitable venture by making nitrites. Oxides of nitrogen are liberated as a concentrated gas stream (50–80% mol NO_X, the rest being water, CO_2) when nitric acid is used to carry out industrial oxidation reactions of organic compounds

$$\text{R-CH}_3 + 2\text{HNO}_3 \rightarrow \text{RCOOH} + 2\text{NO} + 2\text{H}_2\text{O} \quad (93)$$

$$\text{R-CH}_3 + 6\text{HNO}_3 \rightarrow \text{RCOOH} + 6\text{NO}_2 + 4\text{H}_2\text{O} \quad (94)$$

where R is an aromatic group (such as C_6H_4Cl). The abatement, recovery of the NO_X gases, or their value addition in the form of a byproduct can be crucial to the economics of

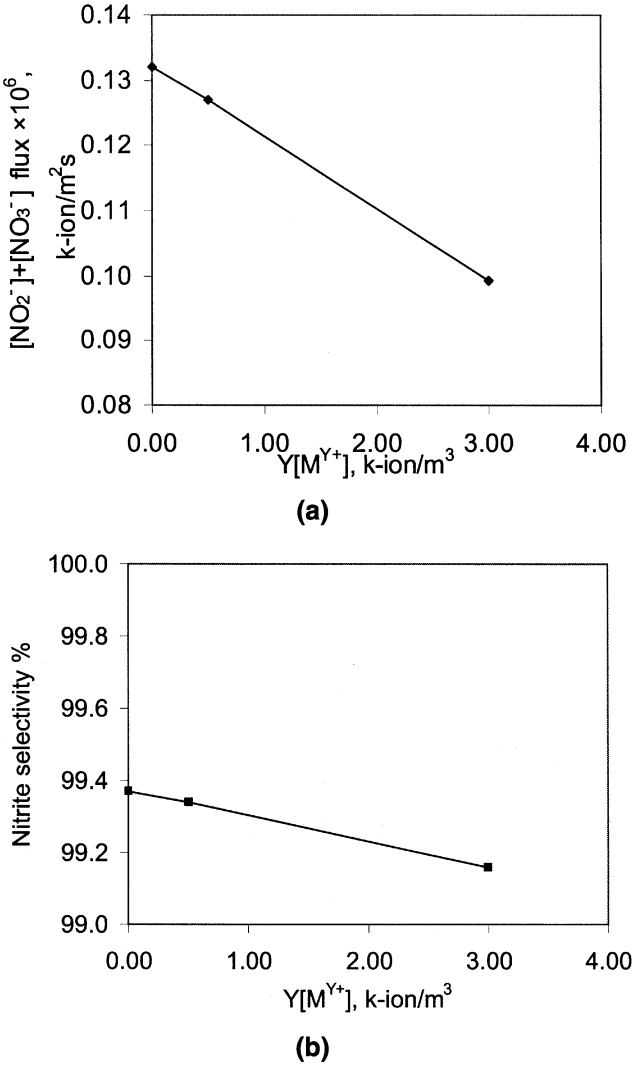

Figure 15. Effect of metal cation concentration on (A) the NO_X removal rate (B) selectivity.

Total $NO_X = 1{,}000$ ppm, $NO^*/NO_2^* = 10$, $T = 328$ K, $P = 1.013 \times 10^5$ N/m^2, $k_G = 0.05$ m/s, $k_L = 1 \times 10^{-4}$ m/s.

the process. Also, $Ca(OH)_2$ is cheaper than NaOH; so, wherever the latter is used to scrub the NO_X gases, it may be worthwhile to use the cheaper reagent $Ca(OH)_2$. However, the deterrent is the low solubility of $Ca(OH)_2$ in water. The upper limit of the $[OH^-]^B$ is the solubility $[OH^-]^{SAT}$. If the condition of $(\lambda/\delta) = 0$ is not maintained, then, the decomposition of HNO_2 leads to lower selectivity and productivity.

Endo and Kusahara (1980) have demonstrated through their patent an ingenious way to make ready-to-use $Ca(NO_2)_2$ solutions by treating the NO_X gases (from ammonia oxidation) in a series of equipment viz., slurry reactor (I), oxidizer, second slurry reactor (II), and filter (Figure 16). Table 7 shows the material balance, which has been established over the system, using the information reported in the patent. This was necessary since some of the stream information was required to be input to the model.

The feeds to the first reactor are: a NO_X rich gas containing 9.5% mol of NO_X, with $NO/NO_2 = 1.2$ and an aqueous

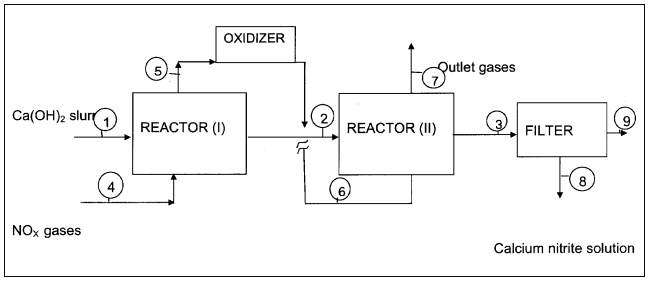

Figure 16. Calcium nitrite process.

slurry of 40% wt $Ca(OH)_2$. Since $Ca(OH)_2$ has low solubility in water, a slurry is maintained to continuously dissolve and supply OH^- to the liquid phase. If the reactor is assumed to be completely backmixed, then the composition of the gas and slurry at the outlet of the reactor will be the same as that of the gas and slurry within the reactor, respectively. The dissolved gases N_2O_3, N_2O_4, HNO_2, HNO_3 react rapidly in the liquid phase. Some formation of HNO_2 takes place from the NO, NO_2, and water in the gas phase also, and the HNO_2 dissolves rapidly into the liquid. This results in the outlet condition (as well as the reactor conditions) posing a higher NO/NO_2 ratio of about 4.31. The high NO/NO_2 ratio favors nitrite selectivity. Whereas the inlet NO_X is 9.5% mol, the reactor operates at 1.6% mol NO_X content in the gas bulk in the backmixed reactor. Due to the lower NO_X content ($\sim 1.6\%$ mol), the rate of NO_X removal is low. The (low) total NO_X content and (high) NO/NO_2 ratio are maintained such that the OH^- ions reach the gas liquid interface ($\lambda = 0$) and prevent HNO_2 decomposition. Thus, conditions for very high selectivity are ensured. Thus, diffusion of $[OH^-]$ ion in the liquid film is not controlling, but gas-phase HNO_2 diffusion and N_2O_3 mass-transfer and liquid-phase hydrolysis are some of the important contributors to nitrite production rate.

In the second reactor, the objective is to consume as much of the NO_X and $Ca(OH)_2$ as possible to achieve clean gas and a solution of calcium nitrite (free of OH^-), respectively. The outlet gases from the first reactor are oxidized to provide a NO/NO_2 ratio of 1.3 to the second reactor. The slurry from the first reactor is fed to the second reactor. The operating point of the second reactor is: outlet $NO_X \cong 0.3\%$ mol. As per the patent, the conditions are maintained such that there is practically no dissolved $Ca(OH)_2$ remaining in the liquid phase so that the filtrate can be marketed directly. This implies that the liquid bulk may contain very low $[OH^-]$, such that $[OH^-]^B/[OH^-]^S \ll 1$. So, the second reactor is operated in such a way that solid dissolution of $Ca(OH)_2$ is limiting. $[OH^-]$ is not available free as such in solution and is continuously reacting upon dissolution. Thus, it is not possible to maintain the condition for $\lambda = 0$. The selectivity in the second reactor is lower (84.76%) The combination of the rates and selectivities of the two reactors gives an overall selectivity of 97.42%.

There are two data points for the estimation of the rate and selectivity corresponding to the operating conditions of each reactor. For the first reactor, operating at close to atmospheric pressure and 328 K, the selectivity was reported in the patent as $\sim 100\%$ and rate of NO_X removal was back-

Table 7. Material Balance Over Patented Calcium Nitrite Process

Stream (Ref. Figure 11)	1	1L	1S	2	2L	2S	3	8	9	4	5	6	7
Phase	S-L	L	S	S-L	L	S	S-L	L	S	G	G	G	G
T, K	328	328	328	328	328	328	330.5	330.5	330.5	448	328	343	330.5
Massflow, kg/h	129.00	95.80	33.20	166.00	159.46	6.54	169	167.31	1.69	246.97		210.13	208.90
Vol. flow m^3/h	0.1124	0.0958	0.0166	0.1214	0.1181	0.0033	0.1181	0.1173	0.00085	328.11	206.65	206.45	207.44
Density, kg/m^3	1147.7	1000	2000	1368	1350	2000	1431	1427	2000	0.753	1.016	0.974	1.000
Molar flow, kmol/h	5.767	5.319	0.449	6.649	6.561	0.088	6.538	6.515	0.023	8.926	7.684	7.669	7.706
Average mol. wt.	22.4	18.0	74.0	25.0	24.3	74.0	25.9	25.7	74.0	27.7	27.3	27.4	27.1
Composition, wt. %													
NO										5.6	1.3	0.9	0.1
NO_2										7.2	0.3	0.7	0.2
O_2										8.0	8.1	7.9	7.8
H_2O	74.2	99.91		67.20	69.96	0	64.75	65.4		9.7	10.6	10.6	12.4
N_2	0				0.00	0	0.00			69.5	79.7	79.9	79.5
$Ca(OH)_2$	25.8	0.089	100.00	4.00	0.06	100	1.00	0	100.00	0.0	0.0	0.0	0.0
$Ca(NO_2)_2$	0			28.80	29.98	0	33.17	33.5		0.0	0.0	0.0	0.0
$Ca(NO_3)_2$	0				0	0	1.09	1.1		0.0	0.0	0.0	0.0
Total	100.0	100.00	100.00	100.00	100.00	100.00	100.00	100.00	100.00	100.0	100	100	100
kmol/h													
NO										0.463	0.100	0.070	0.006
NO_2										0.385	0.023	0.054	0.014
O_2										0.619	0.619	0.604	0.604
H_2O	5.318	5.318	0	6.197	6.197	0	6.079	6.079		1.331	0.813	0.813	0.954
N_2	0.000			0.000			0	0		6.128	6.128	6.128	6.128
$Ca(OH)_2$	0.450	0.00115	0.449	0.090	0.001	0.088	0.023	0.000	0.023	0.000			
$Ca(NO_2)_2$	0.000			0.362	0.362		0.425	0.425		0.000			
$Ca(NO_3)_2$	0.000			0.000			0.011	0.011		0.000			
Total	5.767	5.319	0.449	6.649	6.561	0.088	6.538	6.515	0.023	8.926	7.684	7.669	7.706
Composition mol. %													
NO										5.182	1.306	0.911	0.078
NO_2										4.318	0.303	0.701	0.176
O_2										6.940	8.062	7.879	7.841
H_2O	92.20	99.98		93.204	94.459		92.984	93.310		14.910	10.585	10.606	12.383
N2	0.00	0.00		0.000	0.000		0.000	0.000		68.650	79.744	79.903	79.521
$Ca(OH)_2$	7.80	0.02	100.00	1.349	0.020	100.00	0.349	0.000	100.000	0	0	0.000	0.000
$Ca(NO_2)_2$	0.00	0.00		5.447	5.520		6.495	6.518		0	0	0.000	0.000
$Ca(NO_3)_2$	0.00	0.00		0.000	0.000		0.172	0.172		0	0	0.000	0.000
	100.00	100.00	100.00	100.00	100.00	100.00	100.00	100.00	100.00	100.000	100.000	100.000	100.000

calculated from the patent data (Appendix C). These values needed to be compared with the model predictions. Whenever sufficient details of reactor configuration, impeller type, and so on were not disclosed in the patent, suitable assumptions were made. The inputs to the model were the operating conditions of the reactor (I): such as temperature, pressure, gas and liquid bulk composition, k_G and k_L (see Table 8a). For the reactor (I), the nitrite selectivity calculated by the model is 98.46%, as compared to the value inferred from the patent $\sim$100%. Considering the various uncertainties in the system and the complexity of the model, the match of the model predictions (of rate and selectivity) with plant data can be considered to be "*representative*".

In the case of the reactor I the patent reported the outlet NO_X composition in terms of total NO_X content. The NO/NO_2 ratio could be estimated from the mass balance. The equilibrium gas composition could be specified to the model. In the case of the second reactor, the total NO_X at the gas outlet was known (0.3%) and the NO/NO_2 ratio was arrived at (0.45). Using this value, the predicted nitrite selectivity was comparable with the reported selectivity obtained in reactor II. The specific rate of the NO_X removal in the reactor II was 9.61×10^{-8} k-ion "N"/m^2s, and the value predicted by the model was 1×10^{-7} k-ion N/m^2s, which is quite close. Besides the quantitative comparison in Table 8a, the qualitative interpretation of the statements in the patent and other previous literature have been summarized in Table 8b. Thus, the model is able to explain various practical observations. For a detailed quantitative validation of the model, experimental data from controlled experiments on the NO_x -$Ca(OH)_2$ system are necessary.

Table 8a. Comparison of Model Predictions with Those from $Ca(NO_2)_2$ Patent

Equipment	Value Being Compared	Value Reported in/ Inferred from the Patent	Value Predicted by the Model
Slurry Reactor (I)	Specific rate k-ions "N"/s/m^2	4.75×10^{-7}	3.8×10^{-7}
	Nitrite Selectivity (%)	$\sim$ 100	98.46
Slurry Reactor (II)	Specific rate k-ions"N"/s/m^2	9.68×10^{-8}	1×10^{-7}
	Nitrite Selectivity (%)	84.76	84.75*

*The unknown value of NO/NO_2 at the gas outlet of the 2nd reactor was adjusted to match the selectivity, and the rate prediction was compared.

Table 8b. Explanation of Practical Observations with the Help of Present Model

No.	Experimental/Practical Observation	Ref.	Explanation with Present Model
1(A)	When the reaction is reached to be less than 3 wt. % of the residual $Ca(OH)_2$ content, the formation of the byproduct of $Ca(NO_3)_2$ is increased in the reactor (I)	Endo and Kushahara (1980)	ϵ_S is lower. a_P is lower. Rate of OH^- supply to the liquid phase is lower. The condition of $\lambda = 0$ is no longer maintained. Hence, decomposition of $HNO_2(aq)$ occurs, leading to formation of nitrate.
1(B)	The formation of $Ca(NO_3)_2$ is increased when the nitrogen oxide content in the nitrogen oxide containing gas is high.	Endo and Kushahara (1980)	At a given $[OH^-]^B$, when the NO_X content is higher, then the interface gets more and more acidic and the condition of $\lambda = 0$ is violated, leading to lower nitrite selectivity.
1(C)	When the molar ratio of NO/NO_2 to the inlet of the reactor (I) is less than 1.2, then the formation of byproduct nitrate is greater.	Endo and Kushahara (1980)	For a fixed total NO_X composition, at lower NO/NO_2 ratio, there is greater equilibrium concentration of NO_2, N_2O_4, and HNO_3 in the gas phase. On absorption, this leads to more nitrate in the product.
1(D)	When the molar ratio of NO/NO_2 to the inlet of the reactor (I) is greater than 1.2, then the efficiency of the reaction is low.	Endo and Kushahara (1980)	At high NO/NO_2 ratio, the equilibrium concentration of higher oxides is low, leading to lower rates of absorption.
2	The performance of the NO_x absorption column was enhanced by the presence of increasing hydroxyl ion concentration (up to 2% NaOH) in water; however, at higher concentrations, it was found to be independent of NaOH concentration.	Katima et al. (1992)	Figure 4B shows the increase in the NO_X removal rate with the increase in alkalinity, followed by a level off at higher alkalinity.
3	In case of NaOH solutions, the absorption rate is insensitive to the concentration of NaOH, if it is higher than 0.01 kmol/m^3. The rate decreases remarkably for NaOH concentration smaller than 0.01 kmol/m^3.	Aoki et al. (1982)	Starting from a low value, as the alkalinity increases λ approaches the interface. The extent of HNO_2 decomposition is reduced. Hence, the rate increases noticeably. However, once the interface is alkaline, $\lambda = 0$ condition is continually maintained and there is no further increase in the rate in spite of higher alkalinity.
4	Rate of absorption of NO_2/N_2O_4 in alkaline solution is not very different from that in water.	Newman and Carta (1988)	In water, as well as alkaline solutions, only the forward reaction of N_2O_4 hydrolysis is significant. *(The rate constant k_{35B} as such has a small value. Even during the absorption of N_2O_4 in water, the reverse of hydrolysis reaction is as such slow {as it involves the reaction of three species H^+, NO_3^- and HNO_2}. Therefore, even with the addition of base, rthere is not much of the reverse reaction to inhibit.)* However, in acidic solutions, the reverse reaction may be significant due to higher concentrations of H^+, NO_3^- and HNO_2, and can lower the overall N_2O_4 absorption rate.

Strength and weaknesses of the model

The strength of the model presented here lies in the *unified* approach towards fundamental modeling, which can be used for any multicomponent gas absorption in chemically reacting liquids *over a wide range of pH*. The procedure involves: (a) identification all the species in the gas and liquid phases; (b) writing the differential equations of mass transfer with chemical reaction in the gas, as well as liquid film; (c) providing connecting relations for the gas and liquid concentrations and fluxes at the interface; and (d) the differential equations which contain the terms of forward and backward rates of reactions which attain rapid equilibria (*including water dissociation equilibria*) (simplified by Oleander's (1960) method). It consists of eliminating the complementary rate terms from each pair of diffusion equations and replacing one equation by the equilibrium criterion. (e) Application of the shooting method (*or other numerical method*) to solve the boundary value problem, for arriving at the concentration profiles, rates, and selectivity.

Specifically, in case of NO_X absorption, it does away with the need to use different values of $[H\sqrt{(kD)}]$ of N_2O_3 based on liquid alkalinity and the use of different $[H\sqrt{(kD)}]$ of N_2O_4 at various acid strengths. In the conventional method, the rate of absorption of the NO_X components (N_2O_3, N_2O_4) is expressed in terms of Eq. 1. The reported value of $H\sqrt{(kD)}$ for N_2O_3 varies over a large range in neutral and alkaline solutions and needed experiments to find the lumped parameter $H\sqrt{(kD)}$ at the desired pH. However, the need for experimentation has been reduced by the present modeling exercise since it shows the variation in rates and selectivity with $[OH^-]^B$. The model overcomes the need to use lumped parameters.

The present work reduces the empiricism used in calculation of absorption rates by detailed modeling of the liquid film. This is achieved by considering (a) the interphase equilibria among all the undissociated and dissociated species and (b) kinetic rates of reactions in the liquid film along with other equilibria.

The model provides a physical picture of the happenings near the interface and can help guide the design strategies for various objectives such as high NO_X removal rates, high nitrate yield, high nitrite yield, and so on. The model is generic in nature and can be extended/applied to other cases.

The weaknesses of the model can *lie* in its underlying assumptions. The assumption of two film theory was made for simplicity, but there are many more advanced models to describe mass transfer. A steady-state assumption was made, but the unsteady-state equations can be formulated and solved to get a time-dependent understanding of events at the interface. The latter approach can be useful for the case where contact time is too low to attain steady state, but it is complicated. In terms of the method of solution, the present model needs the tedious use of the iterative Newton Raphson method with low relaxation parameters and good initial guess values of gradients to ensure convergence. Very small grid size on the liquid film side is required to capture the

intricacies of the fast reactions near the interface. In terms of model parameters, these are many in number and their values need to be ascertained over a large range of temperatures. An isothermal condition is a masked assumption. In reality, a temperature profile will develop in the gas and liquid films, depending on the heats of reaction evolved and the thermal conduction and evaporation working towards dispersing the heat. The thirst for better grasp over the subject continues to drive the large efforts in modeling and simulation of NO_X absorption, undeterred by its complexity. In terms of validation, only the $Ca(NO_2)_2$ system was considered since it was the focal point of the present work. Planned experiments can provide complete data necessary for model validation and refinement.

Conclusions

(1) A unified model which depicts the complexities of NO_X absorption over a wide range of pH (3–14) has been formulated and solved.

(2) During absorption, even as N_2O_3 and N_2O_4 get hydrolyzed and almost depleted in the liquid film, their acidic products HNO_2 and H^+ (of HNO_3 and HNO_2) further propagate along the liquid film. If the liquid bulk is acidic, the entire liquid film is acidic. However, if the liquid bulk is alkaline, the acidic components are then neutralized by the alkali at the reaction front λ. The decomposition of HNO_2 in the region $0 < x_L < \lambda$ leads to a fall in selectivity and rate. Therefore, to ensure high nitrite selectivity, the conditions must be chosen such that $\lambda = 0$, that is, the entire liquid film is alkaline.

(3) The NO^*/NO_2^* ratio and the bulk OH^- concentration are the main parameters governing nitrite product selectivity.

(4) Starting from the objective of calcium nitrite process, a fundamental approach led to the development of a generic model to describe NO_X transport phenomena. The model has potential to qualitatively and quantitatively describe the phenomena of NO_X absorption in aqueous solutions over a wide range of pH.

(5) A similar approach can be adopted for various other systems of complex multicomponent absorption in chemically reactive liquids.

Acknowledgment

JAP is most grateful to the Professor M. M. Sharma Fellowship and the Jawaharlal Nehru Memorial Fund for grant of Scholarship.

Notation

a = interfacial area for gas liquid mass transfer per unit dispersion volume, m^2/m^3
d_B = bubble diameter, m
d_P = particle diameter, m
d_{PI} = particle diameter at the inlet, m
D_I = impeller diameter, m
D_J^G = diffusivity of component J in the gas phase, m^2/s
D_J^L = diffusivity of component J in the liquid phase, m^2/s
FERR = error between calculated and specified concentration, $kmol/m^3$
Fr = Froude number
Fl = flow number
g = acceleration due to gravity, m/s
H_D = height of dispersion, m
H_J = Henry's constant for component J, $(kmol/m^3)/(N/m^2)$
$[J(aq)]$ = aqueous phase concentration of component J $kmol/m^3$ or k-ion/m^3
$[J(g)]$ = gas-phase concentration of component J, $kmol/m^3$
JAC = Jacobian matrix
k = rate constant
K = equilibrium constant
k_G = gas side mass-transfer coefficient, m/s
k_L = liquid side mass-transfer coefficient, m/s
k_{SL} = solid liquid mass-transfer coefficient, m/s
M^{Y+} = secondary cation, (Na^+, Ca^{2+}, Mg^{2+}, K^+...)
N = impeller speed, r/s
N_{CD} = critical impeller for complete dispersion, r/s
N_{FL} = impeller speed at flooding, r/s
N_{JSG} = critical impeller speed for solid suspension in presence of gas, r/s
NO* = mole fraction of divalent nitrogen in the gas-phase $y_{NO} + y_{N_2O_3} + 0.5\ y_{HNO_2} - 0.5\ y_{HNO_3}$
NO_2^* = mole fraction tetravalent nitrogen in the gas-phase $y_{NO_2} + y_{N_2O_3} + 2\ y_{N_2O_4} + 0.5\ y_{HNO_2} + 1.5\ y_{HNO_3}$
N_P = power number
N_Q = flow number
P = total pressure, N/m^2
P_C = power consumption, W
P_J = partial pressure of component J, N/m^2
Q_G = gas-flow rate, m^3/s
Q_V = volumetric flow rate of slurry leaving reactor, m^3/s
R = universal gas constant, J/kmol K
R_J = rate of mass transfer of component J, accompanied by chemical reaction, $kmol/m^2s$
Re_P = Reynolds number of particle
Sh = Sherwood number
t = time, s
T = temperature, K
TOL = tolerance
T_R = diameter of the reactor, m
u_T = terminal settling velocity, m/s
V_D = volume of dispersion, m^3
V_G = superficial gas velocity, m/s
V_R = volume of reactor, m^3
V_{SL} = volume of solids + liquid in the reactor, m^3
VG = guess values of concentration gradients, $kmol/m^3/m$
W_I = impeller width, m
x_G = distance (along the gas film), from the gas bulk, m
x_L = distance (along the liquid film), from the interface, m
y = mole fraction

Greek letters

α = parameter
γ = relaxation parameter
δ_G = gas film thickness, m
δ_L = liquid film thickness, m
δ_{VG} = increment if VG, $kmol/m^3/m$
ϵ = fractional holdup
η = selectivity of nitrite/(nitrite + nitrate)
λ = distance of the reaction front {where $[HNO_2(aq)] = 0$} from the interface, m
μ = viscosity, Pa-s
ρ = density, kg/m^3
τ = residence time, s
ϕ = flux from the gas side, crossing the interface, $kmol/m^2s$
ψ = flux from the interface, entering the liquid side, $kmol/m^2s$

Subscripts

F = forward
B = backward
G = gas
J = of component J
L = liquid
S = solid

Superscripts

$*$ = at the interface, pertaining to liquid side
SAT = at saturation
B = bulk
I = at the interface, pertaining to gas side

Literature Cited

Aoki, M., H. Tanaka., H. Komiyama, and H. Inoue, "Simultaneous Absorption of NO and NO_2 into Alkaline Solutions," *J. Chem. Eng. Jap.*, **15**(5), 362 (1982).

Bean, S. L., P. F. Seeling, R. J. Hoffman, and W. W. Low, "Calcium Nitrite Solutions with Low Nitrate Content," U.S. Patent No. 4,285,923 (Aug. 25, 1981).

Brogren, C., and H. T. Karlsson, "A Model for Prediction of Limestone Dissolution in Wet Flue Gas Desulfurization Applications," *Ind. Eng. Chem. Res.*, **36**, 3889 (1997).

Chambers, F. S., Jr., and T. K. Sherwood, "The Equilibrium between Nitric Oxide, Nitrogen Peroxide and Aqueous Solutions of Nitric Acid," *J. Am. Chem. Soc.*, **59**, 316 (1937).

Chandrasekharan, K., and P. H. Calderbank, "Further Observations on the Scale-Up of Aerated Mixing Vessels," *Chem. Eng. Sci.*, **36**, 819 (1981).

Doraiswamy, L. K., and M. M. Sharma, *Heterogeneous Reactions: Analysis, Examples and Reactor Design, Vol. 2*, Wiley, New York (1984).

England, C., and W. H. Corcoran, "The Rate and Mechanism of the Air Oxidation of Parts per Million Concentrations of Nitric Oxide in the Presence of Water Vapor," *Ind. Eng. Chem. Fund.*, **4**(1), 57 (1975).

Endo, M., and K. Kushahara, "Process for Preparing Aqueous Solution of Calcium Nitrite," U.S. Patent No. 4,208,391 (Jun. 17, 1980).

Fukuda, T., K. Idogawa, K. Ikeda, K. Ando, and K. Endoh, "Volumetric Gas Mass Transfer Coefficient in Baffled Horizontal Stirred Vessels," *J. Chem. Eng. Jap.*, **13**(4), 298 (1980).

Gaidis, J. M., and A. M. Rosenberg, "Process for Forming Calcium Nitrite," U.S. Patent No. 4,294,813 (Oct. 13, 1981).

Harnby, N., M. F. Edwards, and A. W. Nienow, *Mixing in the Process Industries*, 2nd ed., Butterworth Heinemann, Oxford (1992).

Katima, J. H. Y., A. Azapagic, and D. Handley, "Nitrogen Oxides Absorption into Sodium Hydroxide Solutions in a Packed Column," *Trans. I. Chem. E.*, **70B**, 39 (1992).

Komiyama, H., and H. Inoue, "Reactions and Transport of Nitrogen Oxides in Nitrous Acid Solutions," *J. Chem. Eng. Jap.*, **11**(1), 25 (1978).

Komiyama, H., and H. Inoue, "Absorption of Nitrogen Oxides into Water," *Chem. Eng. Sci.*, **35**, 154 (1980).

Lefers, J. B., and P. J. van den Berg, "Absorption of NO_2/N_2O_4 in Diluted and Concentrated Nitric Acid," *Chem. Eng. J.*, **23**, 211 (1982).

Lopes de Figueiredo, M. M., and P. H. Calderbank, "The Scale Up of Aerated Mixing Vessels for Specified Oxygen Dissolution Rates," *Chem. Eng. Sci.*, **34**, 1333 (1979).

McCabe, W. L., J. C. Smith, and P. Harriott, *Unit Operations of Chemical Engineering*, McGraw Hill, New York (1993).

Newman, B. L., and G. Carta, "Mass Transfer in the Absorption of Nitrogen Oxides in Alkaline Solutions," *AIChE J.*, **34**(7), 1190 (1988).

Oleander, D. R., "Simultaneous Mass Transfer and Equilibrium Chemical Reaction," *AIChE J.*, **6**(2), 233 (1960).

Peretrutov, A. A., P. P. Kim, N. V. Ksandrov, V. D. Ovchinnikov, and E. N. Kornishina, "Aqueous Solution of Calcium Nitrite," *USSR SU 975,569* (Nov. 23, 1982).

Pradhan, M. P., and J. B. Joshi, "Absorption of NO_X Gases in Aqueous NaOH Solutions: Selectivity and Optimization," *AIChE J.*, **45**(1), 38 (1999).

Press, W. H., S. A. Teulosky, W. T. Vellering, and B. P. Flannery, "Numerical Recipes in FORTRAN the Art of Scientific Computing," 2nd ed., Cambridge University Press, p. 745 (1998).

Rewatkar, V. B., and J. B. Joshi, "Critical Impeller Speed for Solid Suspension in Mechanically Agitated Three Phase Reactors—II: Mathematical Model," *Ind. Eng. Chem. Res.*, **30**(8), 1784 (1991).

Rewatkar, V. B., A. J. Deshpande, A. B. Pandit, and J. B. Joshi, "Gas Hold-Up Behavior of Mechanically Agitated Gas-Liquid Reactors Using Pitched Blade Downflow Turbines," *Can. J. Chem. Eng.*, **71**(2), 226 (1993).

Rowe, P. N., K. T. Claxton, and J. B. Lewis, "Heat and Mass Transfer from a Single Sphere in an Extensive Flowing Liquid," *Trans. Inst. Chem. Eng.*, **43**(1), T14 (1965).

Schwartz, S. E., and W. H. White, "Solubility Equilibria of the Nitrogen Oxides and Oxyacids in Dilute Aqueous Solution," *Adv. Environ. Sci. Eng.*, **4**, 1 (1981).

Shadid, F. T., and D. Handley, "Nitrous Acid Formation and Decomposition During the Absorption of Nitrogen Oxides," *Chem. Eng. J.*, **43**, 75 (1990).

Suchak, N. J., "Computer Aided Design: Absorption of NO_X Gases," PhD Thesis, University of Mumbai, India (1989).

Takakuwa, Y., and F. Arima, "Pure Calcium Nitrite," Japan Kokai 75,102,597 (Aug. 13, 1975).

Takakuwa, Y., T. Funaki, F. Arima, T. Kusahara, and H. Mizuno, "Selective Preparation of Calcium Nitrite," *Japan Kokai*, **76**, 59 (May 25, 1976).

Taylor R., and R. Krishna, *Multicomponent Mass Transfer,* Wiley, New York (1993).

Wendel, M. M., and R. L. Pigford, "Kinetics of Nitrogen Tetroxide Absorption in Water," *AIChE J.*, **4**(3), 249 (1958).

Werner, W., K. Eidam, M. Thiemaan, E. Scheibler, and K. W. Wiegand, "Absorption of NO_2/N_2O_4 in Nitric Acid," *Chem. Eng. Technol.*, **13**, 97 (1990).

Zhantalai, B. P., L. I. Olefir, A. G. Udovenko, N. I. Smalii, I. V. Vokhlov, and A. N. Federov, "Production of Calcium Nitrite," *USSR SU 1,171,417* (Aug. 7, 1985).

Appendix A: Modeling Diffusion Accompanied by Fast Chemical Reactions

On the gas-film side, besides the eight differential equations, there are two constraints of equilibria, which are presumed to hold throughout the gas film due to very fast reactions. Reactions described in Eqs. 3 and 4 are reversible and fast (Lefers and van den Berg, 1982; England and Corcoran, 1975). Hence, it is assumed that instantaneous equilibrium holds under all conditions in case of reactions described in Eqs. 3 and 4 (Newman and Carta, 1988; Shadid and Handley, 1990). Hence, $B' = 0$ and $C' = 0$ in Eqs. 8 and 9

$$\frac{[N_2O_4(g)]}{[NO_2(g)]^2} = \frac{k_{32F}}{k_{32B}} = K_{32} \tag{A1}$$

$$\frac{[N_2O_3(g)]}{[NO(g)][NO_2(g)]} = \frac{k_{33F}}{k_{33B}} = K_{33} \tag{A2}$$

Oleander's (1960) work provides a theoretical basis to model diffusion accompanied by very fast reversible chemical reactions for simple cases. It consists of eliminating the complementary terms from each pair of diffusion equations and replacing one equation by the equilibrium criterion. To eliminate C' from the set of eight gas side equations, Eq. 29 + Eq. 31 gives

$$D^G_{NO}\frac{d^2}{dx_G^2}[NO(g)] + D^G_{N_2O_3}\frac{d^2}{dx_G^2}[N_2O_3(g)] - A' - D' = 0 \tag{A3}$$

To eliminate D' from the set of eight gas side equations, Eq. 29 − Eq. 30 − 2 × Eq. 32 gives

$$D^G_{NO}\frac{d^2}{dx_G^2}[NO(g)] - D^G_{NO_2}\frac{d^2}{dx_G^2}[NO_2(g)] - 2D^G_{N_2O_4}\frac{d^2}{dx_G^2}[N_2O_4(g)] - 2A' + 2M' = 0 \quad \text{(A4)}$$

Thus, the new set of eight equivalent equations is Eqs. A1, A2, A3, A4, 33, 34, 35, and 36. Equations 33–36 are explicit and Eqs. A1–A4 are coupled and need to be solved simultaneously.

On the liquid film side, there are 11 differential equations (Eqs. 37–47) and two equilibrium criteria (Eqs. 24 and 26) to be solved for 11 concentrations. Once again, Oleander's (1960) method is used to eliminate the terms J' and K'. Equation 42 + Eq. 46 gives

$$D^L_{HNO_2}\frac{d^2}{dx_L^2}[HNO_2(aq)] + D^L_{NO_2^-}\frac{d^2}{dx_L^2}[NO_2^-(aq)] + 2H' + I' + \alpha L'/2 = 0 \quad \text{(A5)}$$

Equations 44 + 46 + 47 − 43 gives

$$D^L_{OH^-}\frac{d^2}{dx_L^2}[OH^-(aq)] + D^L_{NO_2^-}\frac{d^2}{dx_L^2}[NO_2^-(aq)] + D^L_{NO_3^-}\frac{d^2}{dx_L^2}[NO_3^-(aq)] - D^L_{H^+}\frac{d^2}{dx_L^2}[H^+(aq)] = 0 \quad \text{(A6)}$$

Thus, the new set of eleven equations for the liquid side are seven explicit equations (Eqs. 37–41, 45, and 47) and the four coupled Eqs. A5, A6, 24, and 26.

Appendix B: Filtering Action of the Gas Film

Let two gases i and j present in a mixture with inert gas z be absorbed in water. In the absence of gas film resistance, the rates of absorption are

$$R_i = k_L\left(H_iP_i^B - 0\right) = k_LH_iP_i^B \quad \text{(B1)}$$

$$R_j = k_L\frac{D_i^L}{D_j^L}\left(H_jP_j^B - 0\right) = k_L\frac{D_i^L}{D_j^L}H_jP_j^B \quad \text{(B2)}$$

Total rate of absorption is:

$$R_T = R_i + R_i \quad \text{(B3)}$$

If selectivity η is defined as R_i/R_T, then

$$\eta = \frac{1}{1 + \frac{D_j^B}{D_i^B}\frac{H_j}{H_i}\frac{P_j^B}{P_i^B}} \quad \text{(B4)}$$

Thus, a lower diffusivity, solubility, and partial pressure of j than that of i will improve selectivity (η) of i. In addition, if there is gas film resistance, then

$$R_i = k_L\left(H_iP_i^I - 0\right) = k_G\left(\frac{P_i^B}{RT} - \frac{P_i^I}{RT}\right) \quad \text{(B5)}$$

$$R_i = \frac{k_LH_iP_i^B}{1 + H_iRT\frac{k_L}{k_G}} \quad \text{(B6)}$$

$$R_j = \frac{k_L\frac{D_j^L}{D_i^L}H_jP_j^B}{1 + H_jRT\frac{k_L}{k_G}\frac{D_j^L}{D_i^L}\frac{D_i^G}{D_j^G}} \quad \text{(B7)}$$

The selectivity η defined as R_i/R_T can be calculated, and will be a function of k_G too. Thus, the gas film resistance acts as a filter.

For simplicity, if the diffusivities of i and j are considered equal, then

$$R_j = \frac{k_LH_jP_j^B}{1 + H_jRT\frac{k_L}{k_G}} \quad \text{(B8)}$$

$$\eta = \frac{R_i}{R_i + R_j} = \frac{1}{1 + \frac{R_j}{R_i}} = \frac{1}{1 + \frac{H_jP_j^B}{H_iP_i^B}\left(\frac{k_G + H_iRTk_L}{k_G + H_jRTk_L}\right)} \quad \text{(B9)}$$

If $k_G \ll H_iRTk_L$ and $k_G \ll H_jRTk_L$ then

$$\eta = \frac{1}{1 + \frac{P_j^B}{P_i^B}} \quad \text{(B10)}$$

If $k_G \gg H_iRTk_L$ and $k_G \gg H_jRTk_L$, then

$$\eta = \frac{1}{1 + \frac{H_j}{H_i}\frac{P_j^B}{P_i^B}} \quad \text{(B11)}$$

Thus, the selectivity changes depending on the magnitude of gas film resistance. This has been called the filtering action of the gas film.

Appendix C: Calculations with Data from Patent

From material balance, the volumetric flow rate of slurry leaving reactor I, $Q_V = 0.1214\ m^3/h = 3.37 \times 10^{-5}\ m^3/s$. Residence time, $\tau = 13$ h (from patent) $= 4.68 \times 10^4$ s.

Volume of (solids + liquid) in the reactor, $V_{SL} = Q_V\ \tau = 0.1214 \times 13 = 1.578\ m^3$.

Guess fractional gas holdup $\epsilon_G = 0.19$ (converged by iterative procedure).

Volume of dispersion, $V_D = V_{SL}/(1 - \epsilon_G) = 1.945\ m^3$.

Assuming ratio of dispersion height: reactor diameter ratio, $H_D/T_R = 1.5$, $T_R = 1.18$ m, $H_D = 1.77$ m.

Area of cross section, $S = \pi/4\ T_R^2 = 1.097$ m^2.

NO_X removal rate = 0.7224 k-ion of N/h (from material balance).

Specific rate of NO_X removal per unit volume of dispersion, $Ra = 0.7224/3600/1.945 = 1.034 \times 10^{-4}$ k-ion/m^3/s.

To compare this rate with the model prediction, it was necessary to specify k_G, k_L, as input to the model. These were calculated as follows. Assume 6 bladed pitched blade turbine up flow impeller for the reactor ($D_I/T_R = 0.5$, $W_I/D_I = 0.3$, $N_P = 2$, $N_Q = 1$). Impeller diameter, $D_I = 0.5^*\ T_R = 0.591$ m. $W_I = 0.3\ D_I = 0.177$ m.

Volumetric flow rate of the gas, Q_G (calculated from patent) = 206.65 m^3/h = 0.057 m^3/s.

Critical impeller speed for flooding is calculated from criterion $Fr = 2$ Fl; gives $N_{FL} = 2.09$ rps.

Assuming operating speed to be 10% higher, $N = 2.31$ rps.

Power consumption, $P_C = N_P \rho_{SL} N^3 D_I^5$; $P_C = 2{,}421$ W.

Specific power consumption, $= 2{,}421/1.945 = 1.2$ KW/m^3.

Solids/slurry (%w) = 4.0, Volume solids/volume slurry = 1.82%.

Solid holdup, $\epsilon_S = 1.82/100^*\ (1 - 0.19) = 0.0147$.

Although the particle diameter can be as fine as 200 μm (2×10^{-4} m) (agglomeration of the particles can lead to $d_{Pi} = 2 \times 10^{-3}$ m. Due to the dissolution of $Ca(OH)_2$ and conversion to $Ca(NO_2)_2$, the outlet particle size is lower, $d_P = 0.0012$ m. $\epsilon_L = 1 - \epsilon_G - \epsilon_S = 0.795$. Assuming spherical particles, $a_P = 6\epsilon_S/d_P = 73.5$ m^2/m^3.

The terminal settling velocity of the particle has been calculated by standard procedure (McCabe et al., 1993) to be $u_T = 0.2$ m/s. The critical speed for solid suspension was worked out (Rewatkar et al., 1991); $N_{JSG} = 2.12$ r/s. The critical speed for complete dispersion was calculated from the correlation by Harnby et al. (1992); $N_{CD} = 0.584$ r/s. The chosen speed N is higher than N_{CD} and N_{JSG} and is acceptable. The gas holdup was calculated from the correlation of Rewatkar et al. (1993)

$$\epsilon_G = 3.54\left(\frac{D_I}{T_R}\right)^{2.08}\left(\frac{N^2 D_I}{g}\right)^{0.51}\left(\frac{Q_G}{N D_I^3}\right)^{0.43}$$

Thus, $\epsilon_G = 0.19$.

The gas-liquid interfacial area was calculated using the correlation of Lopes de Figueiredo and Calderbank (1979)

$$a = 593\left(\frac{P_C}{V_D \epsilon_L}\right)^{0.25} V_G^{0.75}; \qquad a = 217.6 \text{ m}^2/\text{m}^3$$

Bubble diameter, $d_B = 6\epsilon_G/a$; $d_B = 0.0052$ m. The value of $k_L a$ was estimated using the following correlation (Chandrasekharan and Calderbank, 1981)

$$k_L a = \frac{0.0248}{D_I^4}\left(\frac{P_G}{V_D \epsilon_L}\right)^{0.55} Q_G^{0.551/\sqrt{D_I}}; \quad k_L a = 0.094 \text{ s}^{-1}.$$

$k_L = (k_L a)/a = 4.33 \times 10^{-4}$ m/s.

Although there is adequate literature on k_L, it may be pointed out that there is scarce literature/correlations for estimation of k_G in stirred vessels (Fukuda et al., 1980). Based on a preliminary estimate, using $Sh = (k_G d_B/D^G) = 2$, $k_G = 0.0064$ m/s. The value of k_{SL} is estimated using the following correlation (Rowe et al., 1965)

$$Sh = 2.0 + 0.72(Re_P)^{0.5} Sc^{0.333}$$

where

$$Sh = \frac{k_{SL} d_P}{D_B}, \quad Re_P = \frac{d_P u_T \rho_L}{\mu_L}$$

Thus, $k_{SL} = 1.2 \times 10^{-4}$ m/s. The specific rate of NO_X removal per unit gas-liquid interfacial area, inferred from the patent, is $R = (R\underline{a})/\underline{a}$. $R = (1.034 \times 10^{-4}$ k-ion/m^3/s)/(217.6 m^2/m^3) $= 4.75 \times 10^{-7}$ k-ion/m^2/s.

Manuscript received Sept. 20, 2002, revision received Feb. 13, 2003, and final revision received Apr. 5, 2003.